Epitenon-derived cells comprise a distinct progenitor population that contributes to both tendon fibrosis and regeneration following acute injury

Running title: Bi-fated epitenon progenitors in tendon healing

Anne E.C. Nichols[1*], Nicholas W. Wagner[1], Constantinos Ketonis[1], and Alayna E. Loiselle[1]

[1]Center for Musculoskeletal Research, Department of Orthopaedics & Rehabilitation, University of Rochester Medical Center, Rochester, New York

***Corresponding Author**

Anne E.C. Nichols, PhD

Center for Musculoskeletal Research

University of Rochester Medical Center

601 Elmwood Ave, Box 665

Rochester, NY 14642

Phone: (585) 275-4273

E-mail: anne_nichols@urmc.rochester.edu

Acknowledgements: The authors thank the CMSR Histology, Biochemistry and Molecular Imaging (HBMI) Core for technical assistance with preparing samples for histology and the UR Genomics Research Core for assistance with scRNA-sequencing. We would also like to extend our sincere thanks to Yurong Gao, Ph.D. of the Multiphoton and Analytical Imaging Center (MAGIC) Core for her assistance in designing the *in situ* multiphoton imaging experiments.

Funding: This work was supported in part by NIH/NIAMS K99 AR080757 and NIH/NIAMS T32 AR076950 (to AECN) and NIH/NIAMS R01 AR073169 and R01 AR077527 (to AEL). The CMSR HBMI was supported by NIH/NIAMS P30 AR069655.

Author contributions: Study conception and design: AECN, AEL; Acquisition of data: AECN, CK, NWW; Analysis and interpretation of data: AECN, AEL; Drafting of manuscript: AECN; Revision and approval of manuscript: AECN, AEL.

Key words: tendon, epitenon, regeneration, fibrosis, progenitor

SUMMARY

Flexor tendon injuries are common and heal poorly owing to both the deposition of function-limiting peritendinous scar tissue and insufficient healing of the tendon itself. Therapeutic options are limited due to a lack of understanding of the cell populations that contribute to these processes. Here, we identified a bi-fated progenitor cell population that originates from the epitenon and goes on to contribute to both peritendinous fibrosis and regenerative tendon healing following acute tendon injury. Using a combination of genetic lineage tracing and single cell RNA-sequencing (scRNA-seq), we profiled the behavior and contributions of each cell fate to the healing process in a spatio-temporal manner. Branched pseudotime trajectory analysis identified distinct transcription factors responsible for regulation of each fate. Finally, integrated scRNA-seq analysis of mouse healing with human peritendinous scar tissue revealed remarkable transcriptional similarity between mouse epitenon-derived cells and fibroblasts present in human peritendinous scar tissue, which was further validated by immunofluorescent staining for conserved markers. Combined, these results clearly identify the epitenon as the cellular origin of an important progenitor cell population that could be leveraged to improve tendon healing.

INTRODUCTION

Tendons play an essential role in musculoskeletal movement as the means by which muscle contractions are transmitted to bone. Acute tendon injuries occur frequently and heal poorly due to two separate but inextricably linked issues: 1) an exuberant fibrotic healing process that reduces tendon range of motion (ROM) via the formation of peritendinous fibrovascular scar tissue around the injury site and 2) poor intrinsic healing capacity resulting in sub-optimal regeneration of native tendon structure.[1] Injuries to the flexor tendons of the hand are particularly common (more than 300,000 per year[2]) and generate an enormous socioeconomic burden estimated at greater than $400 million per year in the United States.[3] Beyond an initial surgery to restore tendon continuity, up to 24%[4-6] of patients with injured flexor tendons require a second surgical procedure (tenolysis) to remove peritendinous scar tissue and restore ROM, further prolonging patient recovery and increasing the risk of rupture. Despite this significant clinical problem, the ability to design targeted therapeutics to improve tendon healing is severely limited due to a lack of understanding of how various cell populations contribute to the healing process. In particular, the specific identity, origins, and molecular programming of the cells that deposit and sustain the peritendinous scar tissue remain unknown.

Initial work describing flexor tendon healing in canine and non-human primate models identified the epitenon (a thin layer of cells on the surface of tendons) as the primary orchestrator of the early tendon healing response, with epitenon-derived cells thought to contribute to the deposition of collagen in and around the injury site[7-10] and to the production of pro-fibrotic growth factors and cytokines[11] that could potentially contribute to fibrovascular scar formation. Unfortunately, lack of epitenon-specific markers to date has precluded further study of this important cell population. Given the important speculated role of the epitenon as a contributor to the formation of peritendinous adhesions, we sought to identify a genetic driver that could be used to target, track, and manipulate epitenon cells. In particular, we focused on a BAC transgenic mouse line that encodes a tamoxifen (TMX)-inducible Cre (*Cre^{ERT}*) under the control of the *GLAST* [glial high affinity glutamate transporter] (also known as *Slc1a3* or *EAAT1*) promoter.[12] The *GLASTCre^{ERT}* driver has previously been used to

target various types of mesenchymal progenitor cells in other tissues including muscle[13,14] and the spinal cord[15] that ultimately contribute to both the physiological healing process and pathological processes such as fibrosis[15] and heterotopic ossification.[13,14] This particular driver was therefore an attractive candidate for labeling a population with similar purported function in tendon.

In the present study, we identified the *GLASTCre^{ERT}* driver and gene product (GLAST) as a specific marker of epitenon cells in adult mouse and human flexor tendons. We then utilized this new genetic tool to trace the behavior and fate of epitenon-derived cells following acute tendon injury using a combination of genetic lineage tracing and single-cell RNA-sequencing (scRNA-seq) in mice. Surprisingly, epitenon-derived cells were found to contribute not only to fibrotic tendon healing, but also to tendon regeneration in a spatially-dependent manner. Branched pseudotime trajectory and transcription factor enrichment analyses were used to identify potential transcriptional regulators of both fates. Finally, pro-fibrotic epitenon-derived mouse cells were found to be transcriptionally similar to those found in human peritendinous scar tissue, implicating epitenon cells in the formation of function-limiting adhesive scar in human flexor tendon injuries and identifying them as a potential therapeutic target for future study. Combined, these data provide the first in-depth characterization of the epitenon cellular environment and identify the epitenon as a niche for a bi-fated progenitor cell population that contributes to both tendon regeneration and fibrosis following acute injury.

RESULTS

Characterization of the epitenon cellular niche during tendon homeostasis

To determine the targeting of the *GLASTCre^{ERT}* driver during tendon homeostasis, mice were crossed to the *ROSA-Ai9* reporter strain (*GLASTCre^{ERT}; Ai9$^{F/F}$*, referred to as GLAST^{Ai9} mice) which contains the transcript encoding the red fluorescent protein tdTomato downstream of a floxed stop cassette[16] (**Fig. 1A**). Upon tamoxifen (TMX) administration, Cre-mediated recombination causes removal of the stop cassette, allowing permanent expression of tdTomato in all cells expressing *GLAST*, thus labeling them, and all progeny, as GLAST^{Ai9} cells. Intact tendons were examined 14 days after TMX treatment using several imaging modalities (**Fig. 1A**). Sagittal sections through the hind paw demonstrate that GLAST^{Ai9} cells were largely found in a single-cell thick layer lining the surface of both the superficial and deep flexor digitorum longus (FDL) tendons (**Fig. 1B**), consistent with prior characterization of the epitenon structure.[17] Similarly, GLAST^{Ai9} cells were found lining other tendons including the flexor carpi ulnaris tendon in the forelimb, the tendons in the tail, and the Achilles tendon (**Fig. S1A**). A small number of GLAST^{Ai9} cells were also found within the tendon body (**Fig. 1A, 1B**). Previous reports have indicated a small percentage of non-specific recombination using this driver[12,18]; however, no cells were labeled in the epitenon or in the tendon body without exposure to TMX (**Fig. S1B**).

To evaluate the localization of GLAST^{Ai9} cells relative to the collagenous matrix of the tendon, we utilized second harmonic generation (SHG) microscopy. Consistent with the idea that GLAST^{Ai9} cells are located in the epitenon on the surface of the tendon rather than within the tendon itself, GLAST^{Ai9} cells were located outside the tendon matrix (**Fig. 1C**) in the space between the tendon and the adjacent muscle. 3D reconstruction of axial tissue sections taken through the FDL tendon further revealed a distinct boundary between the GLAST^{Ai9} cells on the surface of the tendon and the tenocytes within (**Fig. 1D**). These data also indicate that the *GLASTCre^{ERT}* driver targets multiple cell populations within the epitenon space, including perivascular cells. To further evaluate the cellular makeup of the epitenon niche, we developed an *in situ* multiphoton imaging protocol. Using this

approach, we confirmed the presence of both perivascular and non-perivascular GLAST^{Ai9} cells (**Fig. 1E, 1F**; white arrows) as well as populations of non-GLAST^{Ai9} cells throughout the epitenon (**Fig. 1E, 1F**; yellow arrows). In larger mammals, the epitenon is contiguous with the endotenon which surrounds individual tendon fascicles[17]; however, endotenon in mouse tendons has not been described. Orthogonal views through the FDL tendon *in situ* demonstrate that GLAST^{Ai9} cells are also found in areas between collagen bundles (**Fig. 1G**), suggesting the potential existence of a thin endotenon in mouse flexor tendons.

Due to the presence of a small number of GLAST^{Ai9} cells located within the tendon body (**Fig. 1B, 1C**) we next sought to evaluate the relationship between GLAST^{Ai9} cells and scleraxis (Scx)-expressing tenocytes by generating dual reporter mice to track active *Scx* expression (Scx^{GFP})[19] in addition to labeling GLAST^{Ai9} cells (**Fig. 1H**; GLAST^{Ai9}; Scx^{GFP} mice). GLAST^{Ai9} cells located in the epitenon did not express Scx-GFP (**Fig. 1I**) indicating that this population is distinct from previously described adult Scx-lineage tendon cells.[19,20] A small number (8.7 ± 3%) of GLAST^{Ai9}; Scx-GFP+ tenocytes (**Fig. 1J**) were also observed in the body of the tendon.

In order to better understand the identity of GLAST^{Ai9} cells during tendon homeostasis, we performed single cell RNA-sequencing (scRNA-seq) on uninjured FDL tendons from GLAST^{Ai9} mice. Initial low-resolution clustering revealed five main populations (**Fig. 1K, S1C**): tenocytes (*Scx*+), immune cells (*Adgre1*+), mural cells (*Pecam1*+), muscle cells (*Myod1*+), and a cluster that we subsequently defined as epitenon cells based on the relatively high percentage of GLAST^{Ai9}+ cells in this cluster (**Fig. 1L, S1D**). Confirming our imaging observations, the majority of GLAST^{Ai9} cells (54.7%) were located within the epitenon cell cluster, with smaller numbers found within the tenocyte (39.6%), muscle (2.8%), mural (1.9%), and immune (1.0%) cell clusters (**Fig. 1M**). Similar to our dual reporter (GLAST^{Ai9}; Scx^{GFP}) imaging, a small percentage (3.3%; **Fig. S1E**) of GLAST^{Ai9} tenocytes were found within the tenocyte cluster. Expression of pan-fibroblast markers[21] including collagen types 1 alpha 1 and 2 (*Col1a1* and *Col1a2*), collagen type 5 alpha 1 (*Col5a1*), lysyl oxidase like 1

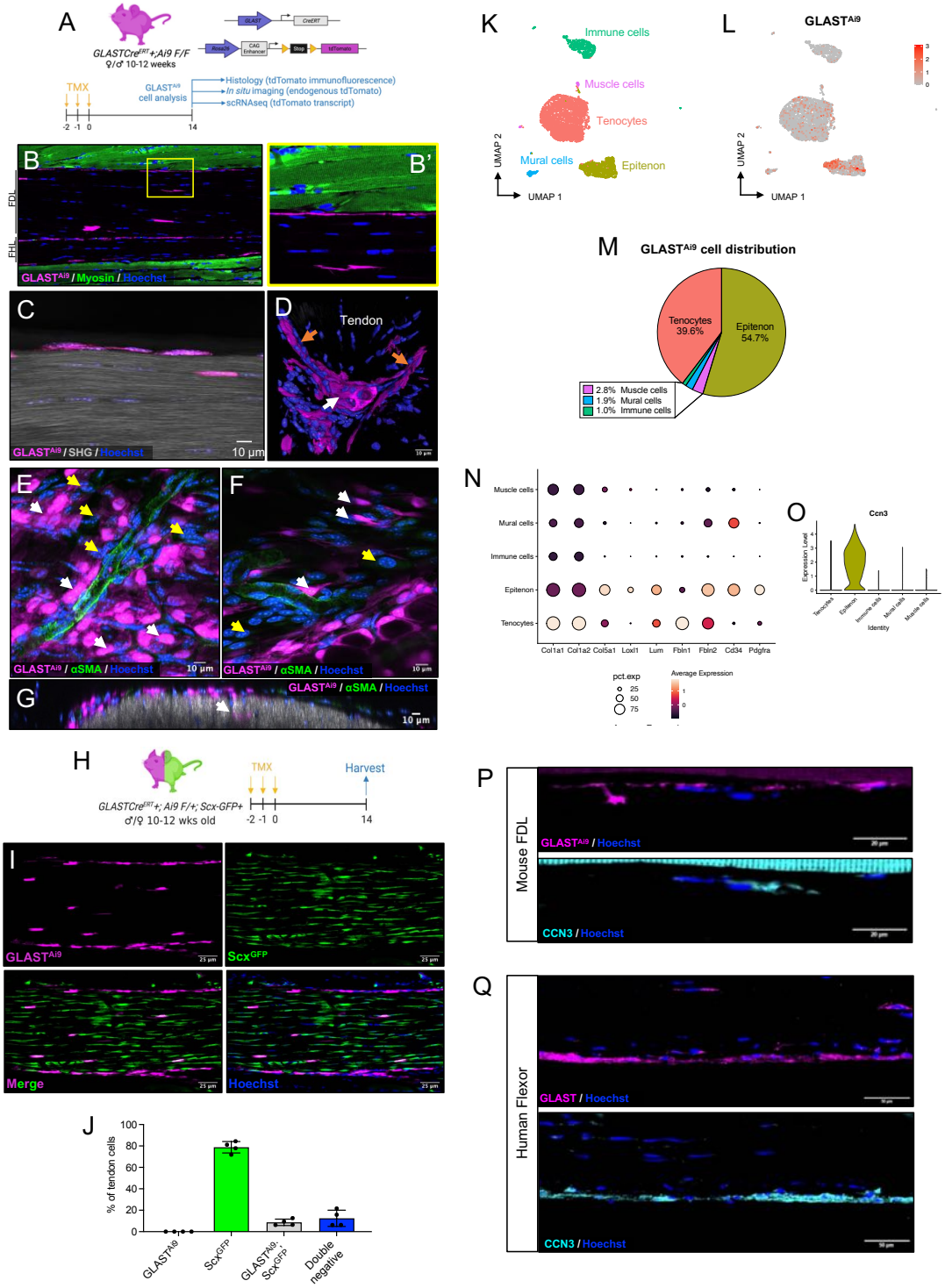

Fig. 1. Characterization of the tendon epitenon during homeostasis. (**A**) Overview of experimental design. (**B**) Sagittal section of the FDL tendon showing IF for GLAST^{Ai9} (magenta) and myosin (green). Scale bar = 50 µm. (**C**) SHG imaging (gray) of endogenous GLAST^{Ai9} labeling (magenta) in relation to the collage matrix in sagittal frozen sections. (**D**) 3D reconstruction of an axial section through the FDL tendon showing GLAST^{Ai9} (magenta) cells in both the epitenon (orange arrows) and surrounding blood vessels adjacent to the epitenon (white arrows). (**E**) *In situ* multiphoton imaging of GLAST^{Ai9} epitenon cells (magenta cells; white arrows), small blood vessels on the surface of the FDL tendon (αSMA; green), and non-GLAST^{Ai9} epitenon cells (yellow arrows). (**F**) *In situ* multiphoton imaging of GLAST^{Ai9} perivascular cells (white arrows) and non-GLAST^{Ai9} cells (yellow arrows). (**G**) Orthogonal view through 3D reconstructed FDL tendon indicating the presence of GLAST^{Ai9} cells (magenta) located between tendon bundles (white arrow). In (**F**) and (**G**), blood vessels are stained with αSMA (green). (**C** - **G**) Scale bars = 10 µm. (**H**) GLAST^{Ai9}; Scx^{GFP} mice received TMX injections and were harvested for frozen histology. (**I**) Sagittal section and (**J**) quantification of endogenous GLAST^{Ai9} (magenta) and Scx^{GFP} (green) fluorescence. Scale bar = 25 µm. Cell populations present (**K**) and clusters containing GLAST^{Ai9} cells (**L**) in scRNA-seq dataset from uninjured FDL tendons. (**M**) GLAST^{Ai9} cell distribution in cell clusters. (**N**) Expression of pan-fibroblast marker genes in clusters from uninjured tendon. (**O**) Epitenon-specific expression of *CCN3*. (**P**) IF of mouse FDL tendons for GLAST^{Ai9} (magenta) and CCN3 (aqua). Scale bars = 20 µm. (**Q**) IF of GLAST (magenta) and CCN3 (aqua) in normal human flexor tendon. Scale bars = 50 µm. Images are representative of n = 2 human tendons. All other images are representative of n = 4-6 mice. In all images, nuclei are counterstained with Hoechst (blue).

(*Loxl1*), lumican (*Lum*), *Cd34*, and platelet-derived growth factor alpha (*Pdgfra*) indicated that epitenon cells are a fibroblast population that is markedly distinct from tenocytes (**Fig. 1N**).

Identification of epitenon-specific markers in adult mouse and human tendons

Given the historic lack of specific epitenon markers, we next interrogated our scRNA-seq dataset to identify candidate epitenon markers for future studies. Expression of communication network factor 3 (*Ccn3*), an extracellular matrix (ECM)-associated signaling protein, was largely restricted to the epitenon cell cluster (**Fig. 1O**). Immunofluorescent (IF) staining in mouse (**Fig. 1P**) and human (**Fig. 1Q**) flexor tendons confirmed that, in addition to GLAST, CCN3 is expressed specifically in the epitenon matrix during homeostasis. Other markers including collagen type 14 alpha 1 (*Col14a1*) and endosialin (*Cd248*) were found to be specific transcriptional markers for the epitenon cluster (**Fig. S1F**). A table containing all epitenon cluster markers can be found in **Supplemental Table 1**.

Epitenon cells proliferate and migrate to the scar area following acute tendon injury

Prior work speculated that epitenon-derived cells are early contributors to the tendon healing response; however, this has yet to be definitively demonstrated. To determine the extent to which epitenon-derived cells participate in tendon healing, GLAST^{Ai9}; Scx^{GFP} mice underwent tendon injury and repair surgery, and tendons were examined at days 3, 7, 10, 14, 21, and 28 post-injury (**Fig. 2A**). GLAST^{Ai9} cells were labeled prior to injury and included a washout period to ensure that only cells expressing GLAST prior to injury were labeled and traced. At day 3 (D3) post-injury, increased numbers of GLAST^{Ai9} cells were observed in the epitenon at the periphery of the injury site (**Fig. 2B**), with expansion of the epitenon through D7. Beginning at D10, GLAST^{Ai9} cells were found both within the newly formed, organized bridging tendon tissue that forms between the cut tendon ends as well

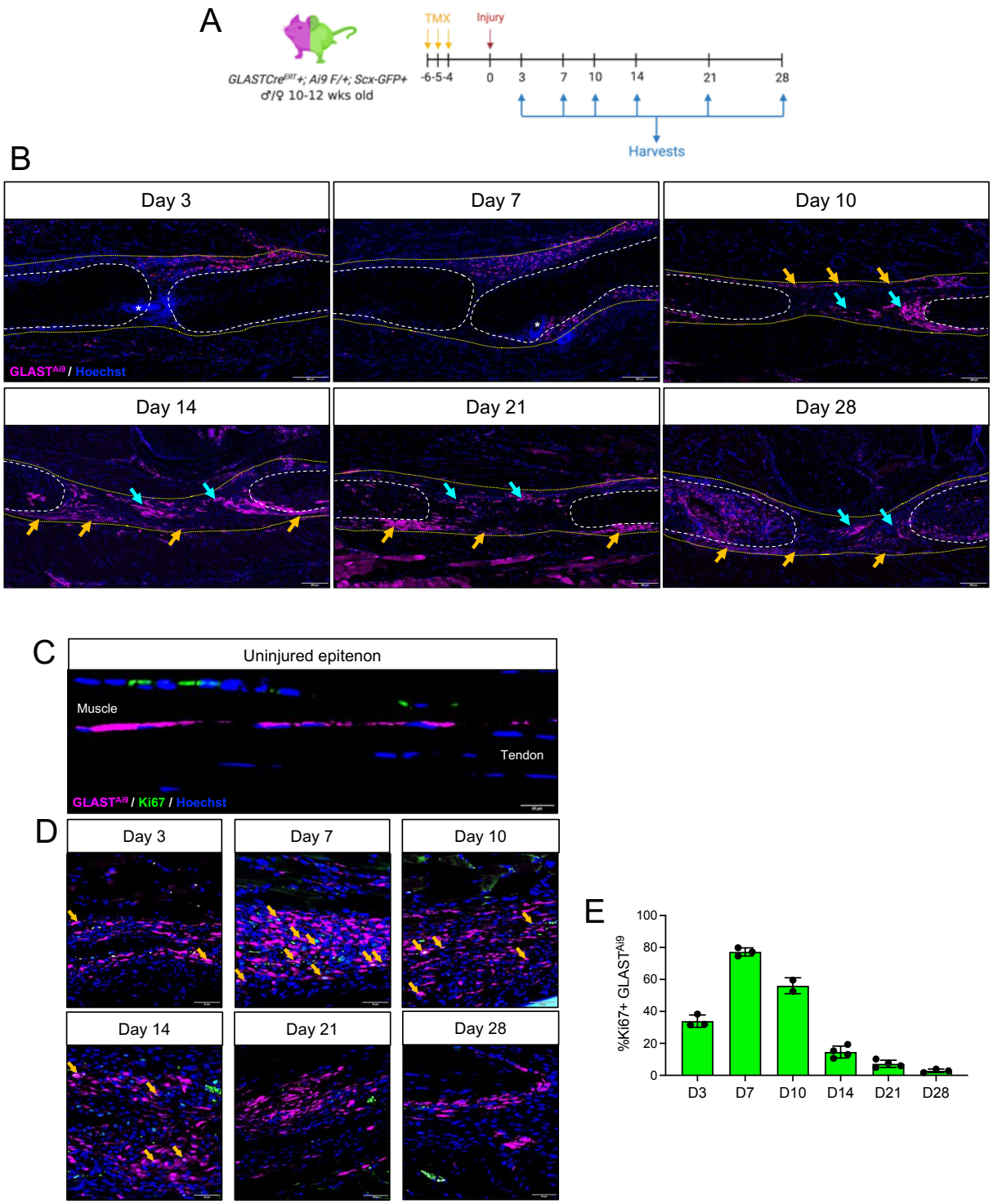

Fig. 2. GLAST^{Ai9} epitenon cells proliferate and migrate into the scar area follow acute tendon injury. (**A**) Overview of experimental design. (**B**) Representative images of GLAST^{Ai9} (magenta) cells located in both a peripheral capsule (orange arrows) around the injury site and within the scar tissue (aqua arrows). Tendon stubs are outlined by white dashed lines and the scar area is outlined by yellow dotted lines. Sutures are marked by white asterisks. Scale bar = 200 µm. (**C**) Ki67 IF (green) in the uninjured epitenon (GLAST^{Ai9}; magenta) and representative images (**D**) of the epitenon adjacent to the injury site throughout healing. (**E**) Quantification of the percentage of proliferating GLAST^{Ai9} epitenon cells (GLAST^{Ai9};Ki67+) at each timepoint. In all images, nuclei are counterstained with Hoechst (blue). All images are representative of n = 2-4 mice per timepoint.

as on the periphery of the injury site. This localization pattern persisted relatively unchanged through at least D28.

Staining for the proliferation marker Ki67 indicated that GLAST^{Ai9} cells do not proliferate in the epitenon during homeostasis (**Fig. 2C**); however, shortly after injury (~D3), Ki67+ GLAST^{Ai9} cells (34.0 ± 3.8%) were observed in the expanded epitenon adjacent to the injury site (**Fig. 2B, 2C**). The number of Ki67+ GLAST^{Ai9} cells in the epitenon peaked at D7 (77.2 ± 2.6%) before declining through D28 (D10: 56.1 ± 5.0%, D14: 14.6% ± 3.7, D21: 7.2 ± 2.3%, D28: 2.8 ± 1.1%). These proliferation dynamics are in contrast to tenocyte proliferation which peaks between D12 and D14 in this model[22], and supports previous suggestions that the epitenon is the primary early responder population following acute tendon injury.

Epitenon-derived cells exhibit spatially-dependent fates

Given the spatially distinct localization of GLAST^{Ai9} epitenon-derived cells (peripheral capsule vs. organized bridging tissue), we next assessed the relationship between GLAST^{Ai9} cells and previously identified tenocyte populations (Scx-GFP+)[20,23,24] throughout healing. Prior to D10, GLAST^{Ai9} and Scx-GFP+ cells in and around the injury site remained largely distinct populations. Interestingly, GLAST^{Ai9}; Scx-GFP+ cells began to appear in the organized bridging tissue at around D10 (**Fig. 3A, 3B**; white arrows), indicating differentiation of GLAST^{Ai9} epitenon cells into tenocytes post-injury. The overall proportion of GLAST^{Ai9}; Scx-GFP+ in the organized bridging tissue increased over time through D28 (**Fig. 3C**). At D28, approximately one-third (33.0% ± 6.7) of the Scx-GFP+ tenocytes in the organized bridging tissue were GLAST^{Ai9} indicating that the epitenon serves as a major source of tenogenic progenitors following injury. Several tenogenic progenitor cell populations that contribute to tendon healing have previously been identified, including melanoma cell adhesion molecule (Mcam; CD146)+ cells[25,26] and alpha smooth muscle actin (αSMA)+ cells.[27] Staining for CD146 (**Fig. S3A**) revealed no GLAST^{Ai9}; CD146+ cells at any point during tendon healing. Similarly, there were no GLAST^{Ai9}; αSMA+ cells within the organized bridging tissue (**Fig. S3B**), suggesting that

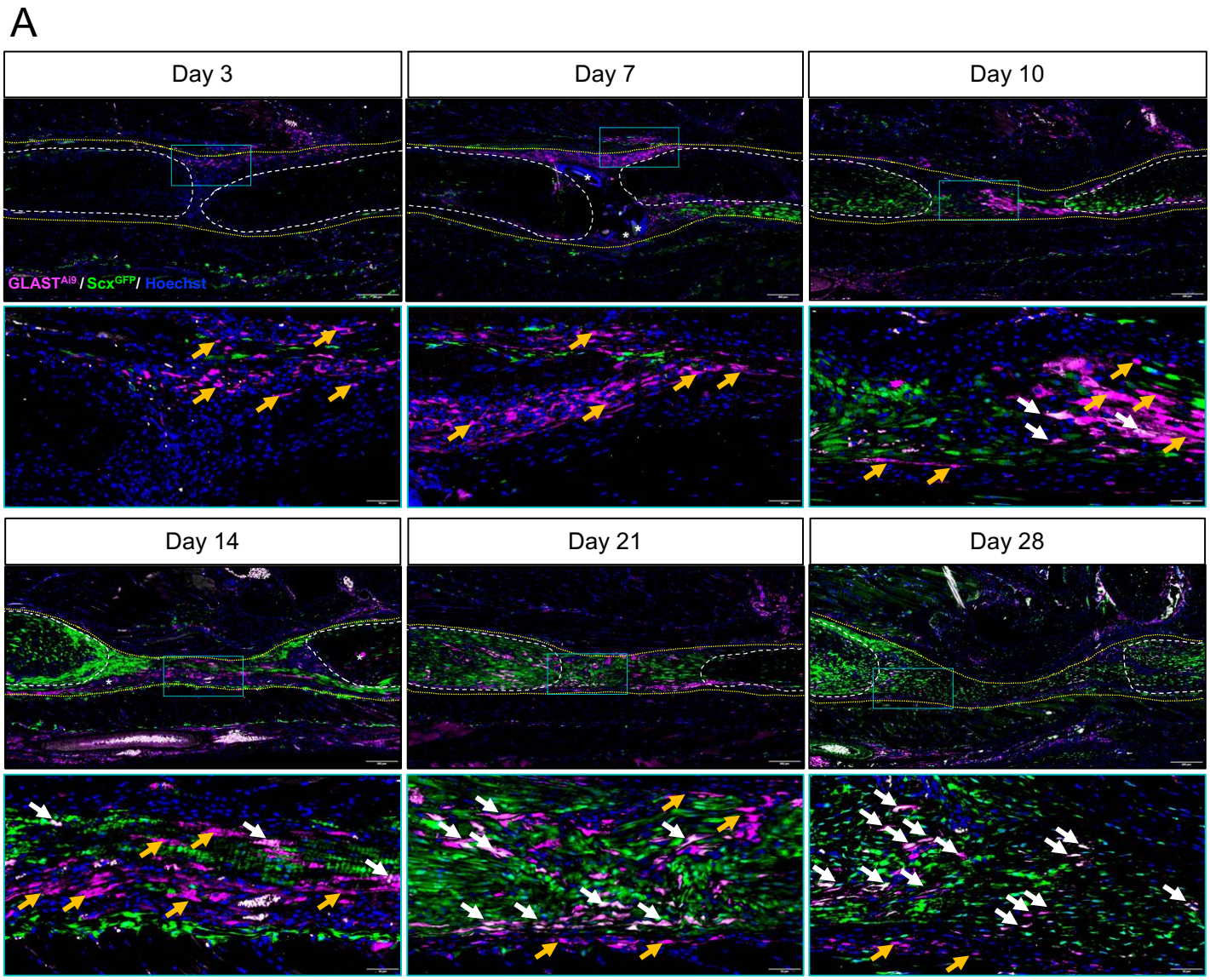

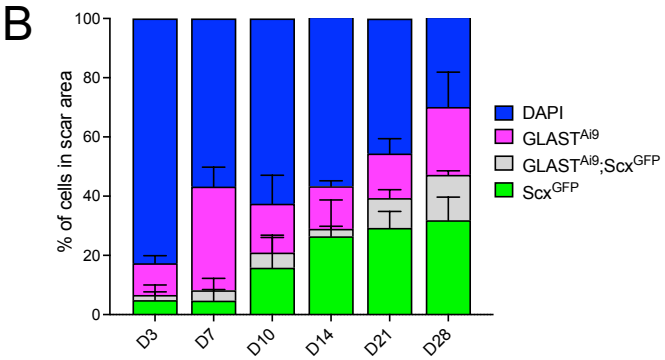

Fig. 3. A subset of GLAST^{Ai9} epitenon cells differentiate into tenocytes during healing. (**A**) Representative images of healing tendons from GLAST^{Ai9}; Scx^{GFP} mice at days 3, 7, 10, 14, 21, and 28 post-injury showing the presence of GLAST^{Ai9}; Scx^{GFP}- cells (magenta cells, orange arrows), Scx^{GFP}+ tenocytes (green cells), and GLAST^{Ai9}; Scx^{GFP}+ tenocytes (white cells, white arrows). Tendon stubs are outlined by white dashed lines and the scar area is outlined by yellow dotted lines. Sutures are marked by white asterisks. Scale bars = 200 μm, magnified image scale bars = 50 μm. (**B**) Quantification of all cell populations present in the scar area throughout healing. In all images, nuclei are counterstained with Hoechst (blue). All images are representative of n = 2-4 mice per timepoint.

GLAST^{Ai9} epitenon cells represent a distinct progenitor pool from those previously described during healing.

In addition to GLAST^{Ai9}; Scx-GFP+ cells in the organized bridging tissue, we observed a persistent band of GLAST^{Ai9}; Scx-GFP- cells in a peripheral capsule surrounding the injury site in the region primarily associated with the formation of fibrotic, peritendinous adhesions[22] from D14 on (**Fig. 3A**; orange arrows). Combined, these lineage tracing experiments suggest two potential fates for epitenon cells post-injury: 2) tenogenic differentiation within the organized bridging tissue or 2) involvement in the formation of peritendinous fibrotic scar tissue.

Single-cell transcriptomic analysis identifies temporally-dynamic contributions of epitenon-derived cells to tendon healing

To better understand the overall role of the epitenon during tendon healing, and with a particular focus on determining the factors regulating potential tenogenic or fibrotic fates of epitenon-derived cells, we performed scRNA-seq on healing tendons from GLAST^{Ai9} mice at 7, 14, and 28 days post-injury. These timepoints were chosen based on our lineage tracing experiments (**Figs. 2 and 3**) and represent points at which key transitional events appeared to occur in epitenon-derived cells: D7 – expansion of the epitenon (large numbers of Ki67+ GLAST^{Ai9} cells), D14 – migration into the fibrotic capsule (GLAST^{Ai9};Scx-GFP- cells) or tenogenic differentiation in the organized bridging tissue (few GLAST^{Ai9}; Scx-GFP+ cells), and D28 – persistence in the fibrotic capsule (GLAST^{Ai9};Scx-GFP- cells) or maturation into tenocytes (increased numbers of GLAST^{Ai9};Scx-GFP+ cells in the organized bridging tissue). To facilitate tracing of the epitenon cells throughout healing, we first integrated the post-injury timepoints with the uninjured dataset described above (**Fig. 4A**) and used the GLAST^{Ai9} genetic label to identify epitenon-derived cells in the integrated dataset (**Fig. 4B**). The integrated dataset captured a wide variety of cell types including several macrophage populations, pericytes, injury-associated fibroblasts (IAF), mural cells, T-cells, and neutrophils which were annotated using canonical markers (**Fig. 4B**). This comprehensive scRNA-seq atlas of tendon healing

will be described in detail elsewhere. For the purpose of this study, we focused our investigation on the clusters containing the largest proportion of epitenon-derived cells (GLAST^{Ai9}). In addition to the epitenon cell cluster (**Fig. 4C**), an increasing proportion of GLAST^{Ai9} cells (uninjured: 4.5%, D7: 26.3%, D14: 38.7%, D28: 38.7%) was also found in a second cluster that was largely absent in the uninjured tendon, but expanded dramatically post-injury (**Fig. 4C**). We surmised that this population most likely represents the newly differentiated, epitenon-derived tenocytes located in the scar tissue given the presence and increasing proportion of GLAST^{Ai9}; Scx-GFP+ cells in this cluster (**Fig. 4C**) and as seen by IF (**Fig. 3**). Based on these observations, we subsequently defined this cluster as the epitenon-derived tenocyte (EDT) cluster. As there were no significantly differentially expressed genes (DEG) between GLAST^{Ai9+} and GLAST^{Ai9-} cells in either the epitenon or EDT clusters (**Fig. S4A**), the fate of each population was examined independent of GLAST lineage for all subsequent analyses.

To characterize the overall contribution of the epitenon and EDT clusters to tendon healing, we examined DEG in each cluster over time (**Fig. S4E-J**). This revealed a generalized healing response in both clusters, with enrichment for biological processes broadly associated with collagen deposition and ECM organization at each timepoint post-injury. Of note, a distinct pro-inflammatory response represented by enrichment for pathways associated with interleukin (IL)-1/ IL-1 beta was observed in the epitenon cell cluster at D7 (**Fig. S4D, S4E**) but was completely absent in the EDT cluster (**Fig. S4K**), suggesting that epitenon-derived cells play a role in initiating the early inflammatory response. To determine cell-type specific functions against this background of general healing, we performed DEG analysis to directly compare the epitenon and EDT clusters at each timepoint. Consistent with the idea of dual fates for epitenon-derived cells, the epitenon cluster displayed significantly higher expression of pro-inflammatory/profibrotic genes, including peptidase inhibitor 16 (*Pi16*), gelsolin (*Gsn*), C-X-C motif chemokine ligand 14 (*Cxcl14*), *Cd248, Cd34,* and *Il6* (**Fig. 4D**), at all timepoints compared to the EDT cluster. Gene ontology (GO) analysis of DEG in the epitenon cluster at D7 post-injury showed enrichment for pathways associated with vasculogenesis, ECM organization, cell adhesion/integrin-mediated signaling, and the insulin-like growth factor signaling pathway (a known

regulator of collagen synthesis in tendon/ligament healing)[28-30] (**Fig. 4E**), supporting a role for epitenon cells as early orchestrators of the healing response beyond an initiation of the inflammatory phase. At D14, epitenon cells were enriched for processes that suggested a shift towards a pro-fibrotic/pro-inflammatory phenotype, including positive regulation of angiogenesis/vasculogenesis, cell adhesion, and inflammatory responses (**Fig. 4F**). At D28, epitenon cells were largely pro-inflammatory, with enrichment for processes including chemokine-mediated signaling, cellular response to IL-1, chemotaxis, inflammatory response, ECM organization, and cellular response to PDGF stimulus (**Fig. 4G**). Given that fibrotic scar formation is thought to be due to the prolonged activity of activated fibroblast populations, the pro-inflammatory phenotype of epitenon cells at D28 (well into the remodeling phase of healing) and enrichment for pathways associated with fibrovascular processes (angiogenesis/vasculogenesis, chemokine-mediated signaling) combined with localization of the periphery of the injury site suggest that epitenon-derived cells are involved in the formation of peritendinous scar tissue.

In contrast to the epitenon cluster, the EDT displayed significantly higher levels of the tenogenic genes *Scx*, tenomodulin (*Tnmd*), Mohawk (*Mkx*), fibromodulin (*Fmod*), thrombospondin-4 (*Thbs4*), and cartilage oligomeric matrix protein (*Comp*) at each timepoint post-injury (**Fig. 4H**). At D7, GO terms were largely associated with glycolysis (glycolytic processes, canonical glycolysis, gluconeogenesis), ECM/collagen fibril organization, and wound healing. The predominance of pathways associated with glycolysis in the EDT is particularly interesting as reliance on glycolysis is known to be one of the mechanisms that preserves stem/progenitor cell pluripotency[31] and suggests that the EDT cluster may represent an uncommitted progenitor. Enrichment for pathways associated with musculoskeletal cell differentiation (bone mineralization and cartilage development) similarly point to the EDT as a priming progenitor cell population at D7. At both D14 (**Fig. 4J**) and D28 (**Fig. 4K**), the EDT cluster was enriched for processes indicative of ECM/collagen fibril organization, musculoskeletal cell differentiation (ossification, endochondral ossification, tendon development,

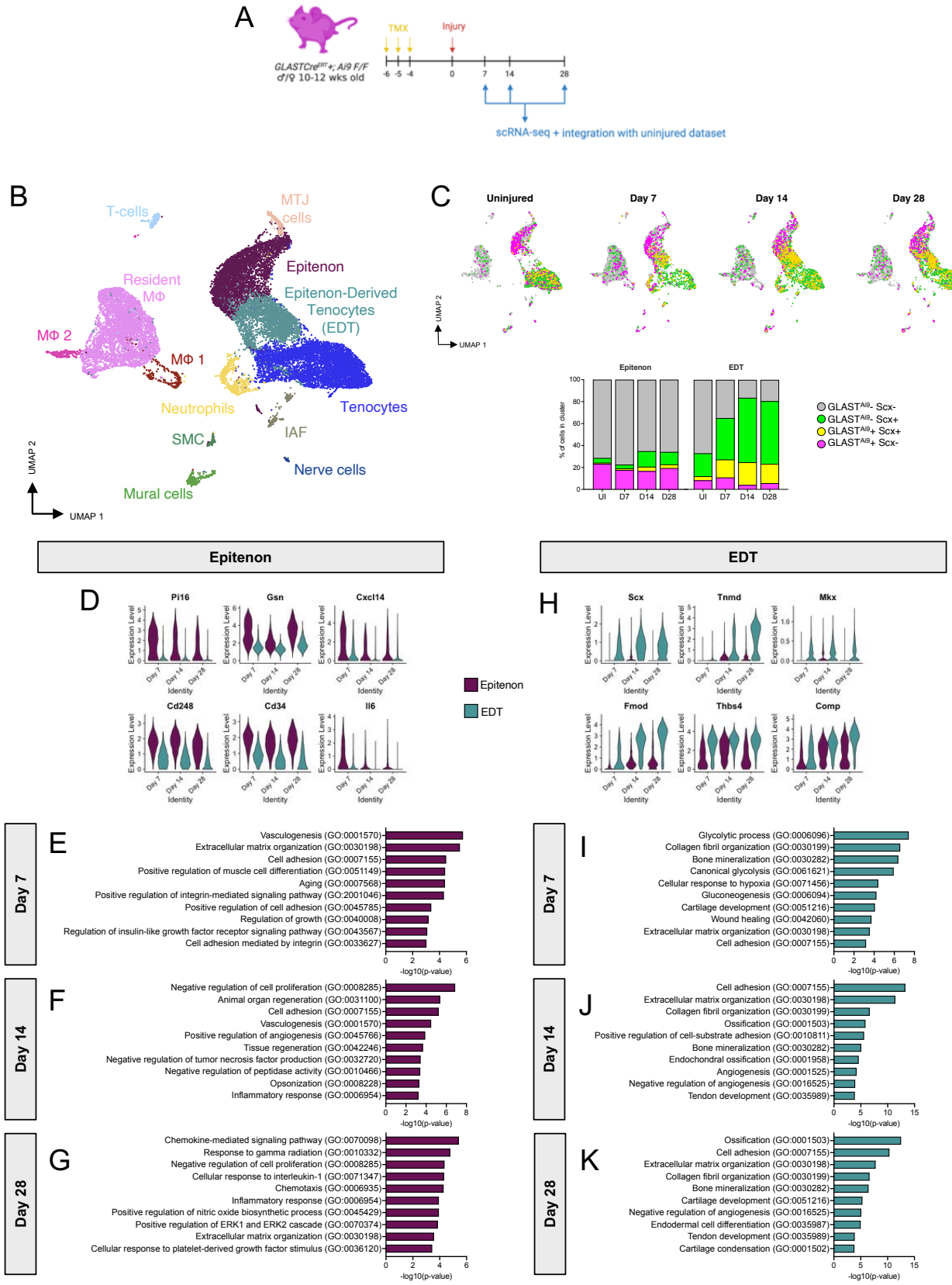

Fig. 4. Epitenon-derived cells exhibit dual fates during healing. (**A**) Overview of experimental design. (**B**) Annotated UMAP plot of integrated healing dataset containing cells from uninjured FDL tendon and tendons at 7, 14, and 28 days post-injury. (**C**) UMAP plots (top) and quantification (bottom) of epitenon cells (magenta: GLAST^{Ai9}+; Scx-), tenocytes (green: GLAST^{Ai9}-; Scx+), and EDT; yellow: GLAST^{Ai9}+; Scx+) in the integrated dataset at each timepoint. (**D** - **E**) Increased expression of fibrotic markers in the epitenon cluster (**D**) and tenogenic markers in the EDT cluster (**E**) over time. (**F** - **K**) GO terms enriched in the epitenon (**F - H**) and EDT (**I** - **K**) clusters at each timepoint.

cartilage development), and negative regulation of angiogenesis, suggestive of a pro-regenerative, tenogenic injury response.

Pseudotime analysis reveals both tenogenic and fibrotic trajectories of epitenon cells

In addition to the inclusion of multiple timepoints in our scRNA-seq analysis, we utilized pseudotime trajectory analysis to better understand the progression of epitenon-derived cells to either a fibrotic or tenogenic fate post-injury. For this analysis, we subset the uninjured epitenon (origin) cluster, the D7, D14, and D28 EDT clusters, and the D7 and D14 epitenon clusters (**Fig. 5A**). The D28 epitenon cluster was removed as it appeared earliest in pseudotime compared to the other post-injury epitenon clusters (**Fig. S5A, S5B**), indicating that in addition to being distinctly pro-fibrotic (**Fig. 4G**), a sizable proportion of epitenon cells at D28 were returning to a more homeostatic state. In support of a fate bifurcation at ~D14, pseudotime trajectory analysis inferred a branched trajectory (**Fig. 5B**) from the uninjured epitenon through the injured epitenon (**Fig. 5C**) to either the D28 EDT (tenogenic) or the D7/D14 epitenon (fibrotic). Correspondingly, tenogenic markers including *Scx*, *Tnmd*, *Mkx*, *Col1a1*, *Fmod*, and growth differentiation factor 5 (*Gdf5*) were significantly upregulated along the tenogenic trajectory (**Fig. 5D**) whereas fibrotic markers including *Cxcl14*, *Pi16*, ADAM metallopeptidase with thrombospondin type 1 motif 15 (*Adamts15*), *Il1b*, chemokine (C-C motif) ligand 6 (*Ccl6*), and collagen type 3 alpha 1 (*Col3a1*) were significantly upregulated along the fibrotic trajectory in pseudotime (**Fig. 5E**). Similar upregulation of tenogenic (**Fig. S5C**) and fibrotic (**Fig. S5D**) marker genes in real-time support the pseudotime lineage reconstruction.

Transcriptional regulation of epitenon-derived cell fates

To gain insight into the factors regulating the tenogenic and fibrotic fates of epitenon cells, we examined gene modules (groups of co-regulated genes) for each trajectory branch. Consistent with tenogenic differentiation from a progenitor cell population, GO term analysis of the tenogenic gene module revealed enrichment for processes associated with musculoskeletal development (*e.g.,*

ossification, skeletal system development, osteoblast and chondrocyte differentiation, bone and cartilage development), collagenous ECM deposition (*e.g.,* ECM organization, positive regulation of collagen biosynthetic process, collagen fibril organization), and cellular response to growth factor stimulus (**Fig. 5F**). Transcription Factor Enrichment Analysis (TFEA) of the tenogenic gene module identified paired related homeobox 2 (*Prrx2*), AE binding protein 1 (*Aebp1*), hes-related family bHLH transcription factor with YRPW motif-like (*Heyl*), odd-skipped related transcription factor 1 (*Osr1*), and *Mkx* as likely transcriptional regulators of the tenogenic fate (**Fig. 5G**). Plotting expression levels of each transcription factor over pseudotime (**Fig. 5H**) indicated that *Prrx2* and *Aebp1* were expressed by uninjured epitenon cells, with steadily increasing expression as cells progress from the uninjured epitenon to the D28 EDT. Expression levels of *Heyl*, *Osr1*, and *Mkx* changed dynamically during tenogenic differentiation, with expression of *Heyl* and *Osr1* peaking in the injured epitenon at D7 and D14 before decreasing. In contrast, expression of *Mkx*, a known regulator of tenocyte maturation[32], peaked in the D14 EDT and remained elevated through D28.

GO term analysis of the fibrotic gene module showed enrichment for biological processes associated with ECM organization/cell-matrix adhesion, pro-angiogenic/neurogenic processes (*e.g.,* positive regulation of angiogenesis, axon guidance, vasculogenesis, nervous system development), and pro-inflammatory processes (*e.g.*, response to cytokine, response to lipopolysaccharide, positive regulation of chemokine production, positive regulation of inflammatory processes), all processes supporting involvement of the epitenon in the formation of fibrovascular scar (**Fig. 5I**). TFEA identified mesenchyme homeobox (*Meox*) 2*, Meox1*, *Osr2*, SRY-box transcription factor 18 (*Sox18*), and FBJ murine osteosarcoma viral oncogene homolog B (*Fosb*) as potential regulators of the pro-fibrotic fate (**Fig. 5J**). Peak expression of *Meox2*, *Osr2*, and *Sox18* early in the fibrotic trajectory suggests that these transcription factors may be involved in the initial, largely pro-inflammatory, response of the epitenon to injury, whereas peak expression of *Meox1* and *Fosb* late in the fibrotic trajectory indicates that they may be promote the switch to a more pro-fibrotic phenotype.

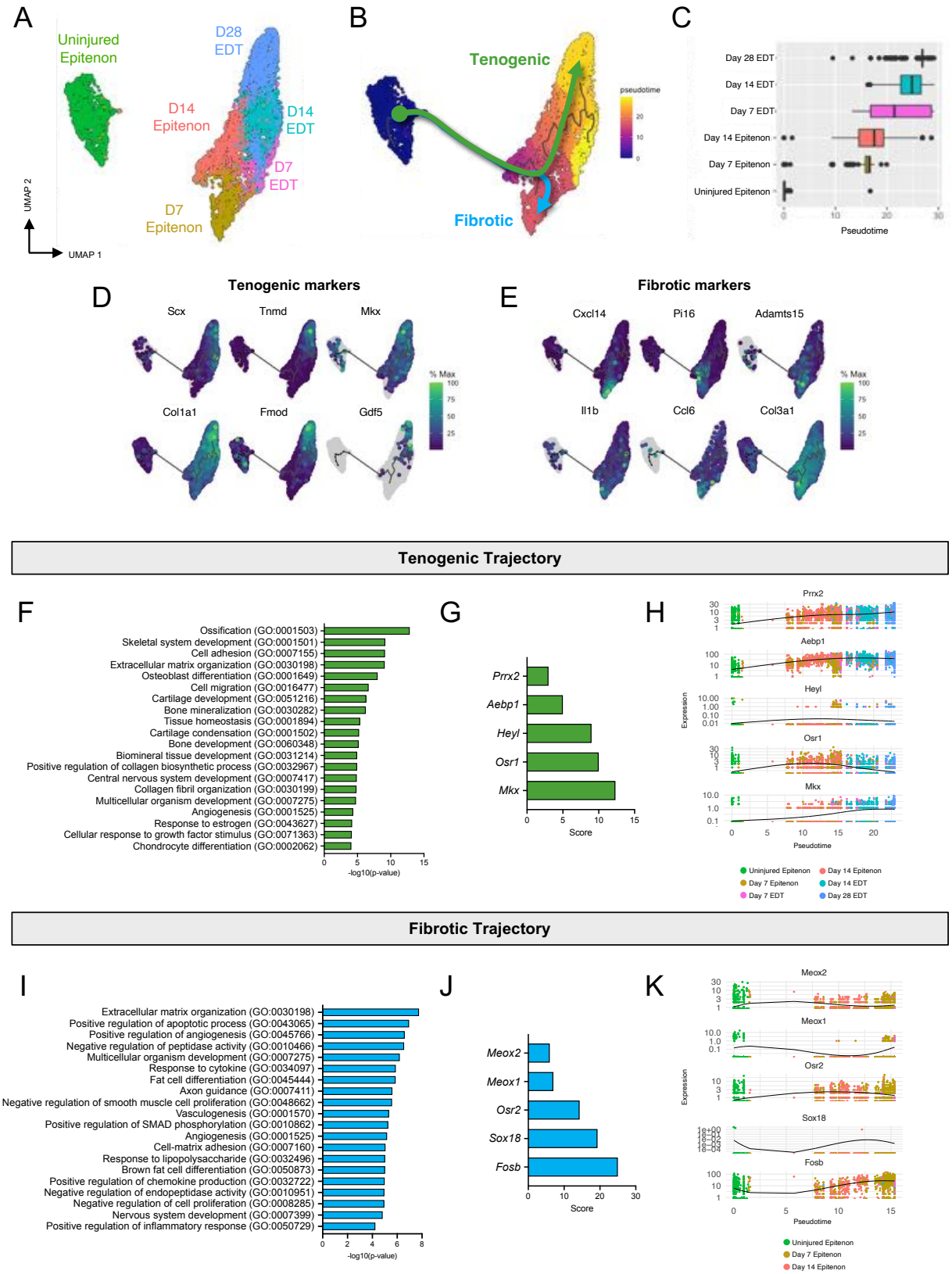

Fig. 5. Branched trajectory analysis and transcriptional regulation of epitenon-derived cell fates. (**A**) Annotated UMAP graph of clusters used for trajectory analysis. (**B**) UMAP depicting inferred branched trajectory from uninjured epitenon to tenogenic (green) and fibrotic (blue) fates. (**C**) Pseudotime progression of epitenon-derived cells from uninjured epitenon to day 28 EDT. (**D** - **E**) Upregulation of tenogenic (**D**) and fibrotic (**E**) markers along the different fate trajectories. (**F**) GO terms enriched along in the tenogenic trajectory. (**G**) Putative transcription factors regulating tenogenesis of epitenon cells. (**H**) Potential tenogenic transcriptional regulators in pseudotime, colored by cell type in real time. (**I**) GO terms enriched along in the fibrotic trajectory. (**J**) Putative transcription factors regulating fibrotic fate of epitenon cells. (**K**) Potential fibrotic transcriptional regulators in pseudotime, colored by cell type in real time.

Human peritendinous adhesion cells are transcriptomically similar to pro-fibrotic mouse epitenon cells

In order to determine the relationship between epitenon-derived pro-fibrotic cells in our mouse model and the cell populations present in mature human peritendinous scar, we integrated our mouse healing dataset with a scRNA-seq dataset derived from human flexor tendon peritendinous scar tissue removed during tenolysis surgery. First, cell populations in the human dataset were annotated based on established markers (**Fig. S6A**). The mouse healing integrated UMAP was then used as a reference and human cells were mapped to their corresponding mouse clusters (**Fig. 6A**). The majority of cells in the human scar tissue mapped to the mouse smooth muscle cell cluster (54%; **Fig. 6B**) which is consistent with the highly vascular nature of human peritendinous scar tissue. The second highest percentage (23.2%) of cells in the human scar tissue mapped to the mouse epitenon cluster. More specifically, the majority of human cells that mapped to the mouse epitenon cluster further identified with the mouse epitenon at D14 (9.6%) and D28 (11.23%), suggesting that the majority of the fibroblasts present in human peritendinous scar tissue are transcriptionally similar to the pro-inflammatory/pro-fibrotic mouse epitenon cells.

Finally, to determine whether human scar cells may be derived from epitenon cells, we interrogated the mouse scRNAseq-dataset for epitenon-specific markers that where conserved throughout healing. *Ccn3* is not only expressed specifically in the epitenon during homeostasis (**Fig. 1O-Q),** it is also expressed by mouse epitenon cells throughout healing (**Fig. S6A**) and by fibroblasts present in human peritendinous scar tissue (**Fig. S6B**). Staining for CCN3 in scar tissue from three different tenolysis patients revealed the presence of CCN3+ cells throughout. Combined, these data suggest that the fibroblasts present in established human peritendinous scar tissue may originate from the epitenon.

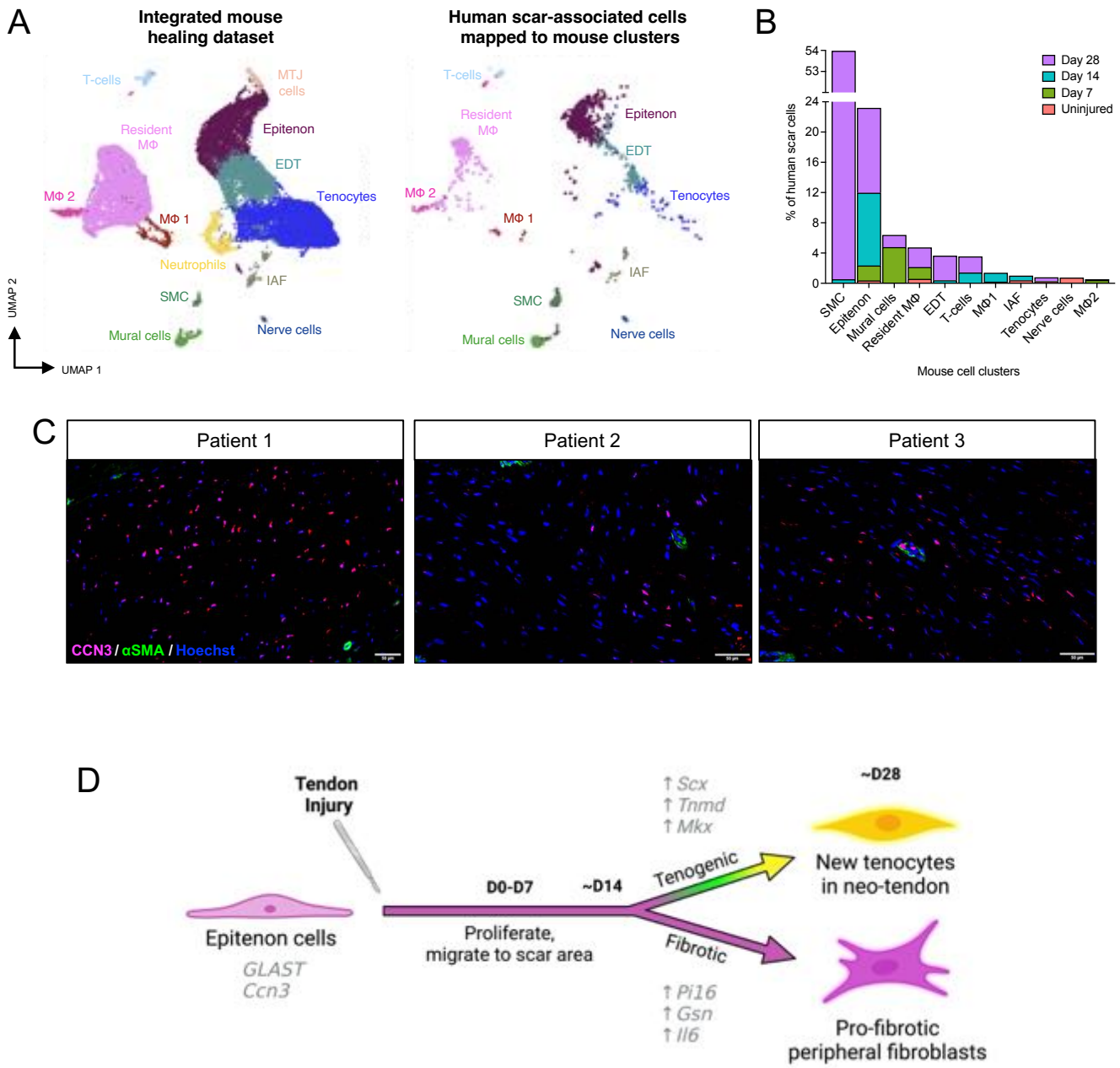

Fig. 6. Integration of mouse healing scRNA-seq dataset with human peritendinous scar tissue. (**A**) Annotated UMAP graphs of human peritendinous scar-associated cells (right) mapped to the integrated mouse healing scRNA-seq atlas (left). (**B**) Proportion of human peritendinous scar-associated cells that correspond to individual mouse clusters, colored by timepoint. (**C**) Immunofluorescent staining for conserved epitenon-derived cell marker CCN3 in the peritendinous scar tissue from three individual human patients. (**D**) Working model of the epitenon-derived cell contribution to tendon healing.

DISCUSSION

Understanding the specific identity, origin, and fate of the various cell populations that contribute to tendon healing is vital to the development of targeted therapeutics to improve the naturally poor healing response of tendons. Here, we report an in-depth spatial and temporal characterization of the epitenon-derived cellular contribution to tendon healing and identify the epitenon as a niche for a bi-fated progenitor cell population that participates in both tendon regeneration and peritendinous fibrosis post-injury. Integrated scRNA-seq analysis of mouse tendon healing with human peritendinous scar tissue found striking transcriptional similarity between pro-fibrotic mouse epitenon cells and the fibroblasts present in human scar tissue, implicating the epitenon as a major contributor to the formation of peritendinous fibrosis. Combined, these data establish the epitenon as the cellular origin of an important progenitor cell population that could be leveraged to improve overall tendon healing via modulation of both peritendinous scar formation and regeneration of the tendon itself (**Fig. 6D**).

The goal of this study was to identify a specific genetic driver that could be used to determine the epitenon cell contribution to the formation of peritendinous adhesions following acute tendon injury. To that end, we have established the *GLASTCre*^{ERT} driver as a tool to target the epitenon in adult mice and identified both GLAST and CCN3 as conserved epitenon-specific markers in mice and humans during both homeostasis and throughout healing. This finding will greatly enhance future work to understand the overall cellular landscape of tendon healing across models. In addition, GLAST^{Ai9} epitenon cells localize to the peripheral scar tissue during murine tendon healing and have a distinctly pro-inflammatory/pro-fibrotic transcriptomic profile that was highly similar to that of fibroblasts isolated from human peritendinous scar tissue. Combined, these results suggest that the epitenon plays an integral role in the development of peritendinous adhesions.

Surprisingly, in addition to being a source of pro-fibrotic cells during healing, GLAST^{Ai9} epitenon-derived cells also underwent tenogenesis in the organized bridging tissue post-injury, indicating that the epitenon serves as a niche for a bi-fated progenitor cell population. Previous

studies have identified a number of adult tenogenic progenitor cell populations derived from various parts of the tendon that participate in tendon healing, including those derived from the tendon sheath/paratenon (*αSMA*+[27], *Tppp3*+[33], and *Bglap*+[34]) and parenchyma (*Axin2*+[35,36], *Scx*+[20,37]). The degree to which these populations are specific to different compartments varies across tendons: for example, *Tppp3* is a sheath/paratenon-specific marker in the patellar tendon but not in the Achilles[35,38] or FDL tendons (data not shown). Moreover, while most tendons are extrasynovial (including the non-digit portion of the FDL), all tendons have an epitenon. As such the epitenon is a more uniformly-available source of tenogenic progenitors and thus likely plays a larger role in tendon regeneration than sheath/paratenon-derived cells. Interestingly, similar temporal and spatial behaviors are observed in all tenogenic progenitors cell populations across tendon types and injury models described to date, including early proliferation and migration in the injury site (~D7) before tenogenic differentiation (~D14).[27,33-35] This suggests a common post-injury tenogenic trajectory regardless of cellular origin; however, it remains unclear whether these populations undergo the same degree of tenogenesis or have equivalent functional roles during healing. Additional work is required in order to determine whether all progenitor populations are required for tendon healing or if a particular population may represent a more attractive therapeutic target to improve tendon regeneration in specific tendons or injury types.

The GLAST^{Ai9} epitenon-derived cells identified in this study are unique among tendon progenitors in that they appear to function in both a pro-fibrotic and pro-tenogenic manner depending on their spatial localization. Previous work has focused on improving tendon healing by promoting the recruitment and differentiation of endogenous progenitor cell populations; however, equally important to a superior tendon healing response is the ability to decrease peritendinous scar formation. The dual fate of epitenon-derived cells is therefore an important cellular trajectory to understand, and unraveling the transcriptional networks regulating both fates could facilitate targeted intervention to simultaneously suppress pro-fibrotic activities and promote tendon regeneration through improved tenogenesis. While progress has been made understanding transcriptional regulation of tenogenic

progenitors during development[39,40], less is known about the transcriptional networks driving adult tenogenic progenitor differentiation. In this study, we identified *Prrx2*, *Aebp1*, *Heyl*, *Osr1*, and *Mkx* as potential key transcription factors regulating the tenogenic trajectory of epitenon-derived cells in the organized bridging tissue post-injury. With the exception of *Mkx*, the expression patterns and functions of these transcription factors have not been extensively characterized in tendon. While *Scx* is the earliest known marker of tenocytes[41,42], *Mkx* has been shown to play a crucial role in tenocyte maturation later during embryonic development.[32] In our study, *de novo* expression of *Scx* in epitenon-derived tenogenic progenitors began early (~D7) post-injury, with *Mkx* expression increasing at later timepoints (D14-D28) indicating a conserved role for *Mkx* in tenocyte maturation during adult tenogenesis. Expression of *Prrx2* and *Aebp1* has been reported in both embryonic mesenchymal cells and developing tendons.[43,44] Consistently, we observed increasing expression of both transcription factors along the tenogenic trajectory, suggesting common regulation of early progenitor cell differentiation in both embryonic development and adult healing. *Osr1* is also expressed by mesenchymal cells during development, however, overexpression of *Osr1* can repress tenocyte differentiation.[45] Sharp downregulation of *Osr1* expression just prior to tenogenic differentiation of epitenon cells (~D14) in our model is consistent with a similar role for *Osr1* in adult healing. We are unaware of any studies examining the expression of *Heyl* in tendon development or tenogenic differentiation, therefore its identification as a potential tenogenic regulator during adult tendon healing warrants further investigation. Combined, these data suggest that post-injury tenogenic progenitor cell differentiation is largely regulated by similar transcriptional networks as embryonic tendon development and identify novel transcriptional regulators for future study.

In addition to transcriptional regulators of epitenon-derived cell tenogenesis, we identified potential transcription factors involved in the pro-fibrotic activities of epitenon-derived cells in the peripheral scar tissue. Interestingly, many of the transcription factors identified in our study have been shown previously to be involved in the development of fibrosis in other tissues but have not been studied in tendon. Both *Meox1* and *Meox2*, are known to play central roles in mediating transforming

growth factor beta (TGFβ)-induced fibroblast activation and subsequent pro-fibrotic activity in human heart, lung, kidney, and liver fibroblasts.[46-48] Additionally, *Meox2* can modulate nuclear factor-kappaB (NF-κB) signaling through direct binding with both p65 and IKKβ.[49] Increased expression of *Meox2* along the pro-fibrotic trajectory of epitenon-derived cells post-injury is therefore consistent with previous work from our lab identifying NF-κB signaling as a potent pro-fibrotic regulator during tendon healing.[50,51] In addition to *Meox1* and *Meox2,* expression of *Fosb* was also increased in pro-fibrotic epitenon-derived cells. *FosB* has been shown to stimulate expression of the pro-fibrotic matricellular proteins connective tissue growth factor (CTGF) and tenascin-C[52], both of which are associated with fibrosis in tendon and other tissues.[53-55] The potential role of *Sox18* in tendon fibrosis is less clear. *Sox18* is most widely characterized in the context of vascular development where it promotes endothelial cell differentiation.[56] Studies have also linked elevated expression of *Sox18* to increased cancer cell metastasis[57], indicating that it may promote a more proliferative, migratory cell phenotype. Similarly, *Osr2* is known to regulate cell proliferation in many cell types, including mesenchymal stem cells[45] and osteoblasts.[58] Peak expression of *Sox18* and *Osr2* in the early pro-fibrotic trajectory in our study suggest that they may play a role in promoting epitenon cell proliferation and migration; however, this remains to be determined.

This study demonstrates the power of combined lineage tracing and scRNA-seq to gain unprecedented insight into both cellular behavior and the transcriptional mechanisms regulating those responses. In addition, the combined use of clinically-relevant animal models with patient-derived samples highlights the enormous potential to identity novel markers and translational mechanisms that would not be possible using human tissue alone. For example, despite the recent proliferation of scRNA-seq studies using human tendon[59-61], annotation of distinct cell clusters has remained difficult due to a lack of specific markers for various tendon cell populations. In particular, lack of an epitenon cell marker has meant that this important structure has been entirely excluded from human transcriptomic studies. Here, through dual species scRNA-seq analysis, we uncovered epitenon-specific markers that can be used to annotate the epitenon in future investigations. Additionally,

through analysis of conserved markers for pro-fibrotic epitenon-derived cells, we identified epitenon-derived cells as a novel cellular therapeutic target to reduce peritendinous adhesion formation in humans following acute flexor tendon injures.

In summary, these data identify the epitenon as a source of bi-fated progenitor cells that contribute to both tendon fibrosis and regeneration in mice. Moreover, we provide evidence that this role is partially conserved in human tendon healing, as epitenon-specific markers were present in a small cohort of patient-derived peritendinous scar tissue. Identifying the specific role of the epitenon in tendon healing as well as the molecular mechanisms and transcriptional networks driving these responses is a significant step towards the ultimate goal of improved tendon healing through the suppression of adhesion formation and promotion of tendon regeneration.

Limitations of the study

The main limitation of this relates to the use of the *GLASTCre*^{ERT} driver for lineage tracing experiments. Both *in situ* imaging and scRNA-seq in intact mouse flexor tendons showed that not all epitenon cells are targeted by the *GLASTCre*^{ERT} driver and therefore only a subset of epitenon cells are able to be identified spatially during tendon healing. Additionally, the *GLASTCre*^{ERT} driver targets several non-epitenon cell populations, including adipocytes, perivascular cells, and macrophages, therefore we cannot rule out the contribution of extrinsically-derived GLAST^{Ai9} cells to the tendon healing process by lineage tracing alone. To overcome this, we combined genetic lineage tracing with scRNA-seq which facilitated identification of both epitenon- and epitenon sub-population-specific markers. Future investigations utilizing novel Cre drivers generated using these markers will further clarify the specific functional roles of all epitenon cell populations to tendon healing.

METHODS

Resource Availability

Contact for Reagent and Resource Sharing

Further information and requests of reagents can be directed to and fulfilled by the Lead Contact, Anne Nichols (anne_nichols@urmc.rochester.edu).

Materials Availability

This study did not generate new unique reagents.

Data and code availability

Single-cell RNA-sequencing data have been deposited at GEO and are publicly available as of the date of publication. Accession numbers are listed in the key resources table. Microscopy data reported in this paper will be shared by the lead contact upon request. This paper does not report original code. Any additional information required to reanalyze the data reported in this paper is available from the lead contact upon request.

Experimental model and subject details

Animal Ethics

All experiments were carried out in strict accordance with the recommendations in the Guide for the Care and Use of Laboratory Animals of the National Institutes of Health. All animal procedures were approved by the University Committee on Animal Research (UCAR) at the University of Rochester. Mice were kept in standard housing conditions throughout breeding and experimentation.

Mice

GLASTCre^{ERT} (STOCK Tg[Slc1a3-cre/ERT]1Nat/J; #012586)[12] and *ROSA-Ai9* (B6.Cg-Gt[ROSA]26Sortm9[CAG-tdTomato]Hze/J; #007909)[16] mice were obtained from The Jackson

Laboratory (Bar Harbor, ME, USA). *Scleraxis (Scx)-GFP* (Tg[Scx-GFP]1Stzr/Tg[Scx-GFP]1Stzr; referred to as Scx^{GFP})[62] reporter mice were generously provided by Dr. Ronen Schweitzer (Oregon Health Sciences University). To identify and trace GLAST-lineage cells by immunofluorescence and scRNA-seq, *GLASTCre*^{ERT} mice were crossed to the *ROSA-Ai9* strain to generate experimental animals (*GLASTCre*$^{ERT+}$*; Ai9*$^{F/F}$: referred to as $GLAST^{Ai9}$). Male and female mice $GLAST^{Ai9}$ mice (10-12 weeks old) received three i.p. injections of tamoxifen (TMX; 100 mg/kg in corn oil, T5648 and C8267, Sigma Aldrich, St. Louis, MO, USA) and tendons were harvested 14 days after the final injection. To evaluate potential tenogenic differentiation of GLAST-lineage cells, $GLAST^{Ai9}$ mice were crossed to Scx^{GFP} mice (*GLASTCre*^{ERT}*; Ai9*$^{F/+}$*; Scx*$^{GFP+}$: referred to as $GLAST^{Ai9}$; Scx^{GFP}) which allows tracking of cells that actively express the tenogenic transcription factor scleraxis (*Scx*). $GLAST^{Ai9}$; Scx^{GFP} mice received the same TMX regimen described above for $GLAST^{Ai9}$ mice.

Flexor tendon injury model

To trace $GLAST^{Ai9}$ epitenon cells, male and female $GLAST^{Ai9}$ and $GLAST^{Ai9}$; Scx^{GFP} mice (10-12 weeks old) received three i.p. TMX injections beginning seven days prior to flexor tendon injury, allowing a four-day TMX washout period. This labeling regimen ensured that only cells expressing GLAST prior to injury were labeled and that no subsequent labeling occurred during tendon healing. Mice then underwent complete transection and repair of the flexor digitorum longus (FDL) tendon in the hind paw as previously described.[22,24,50,63-65] Briefly, mice were anesthetized with Ketamine (100mg/kg) and Xylazine (10mg/kg) and sustained-release buprenorphine (ZooPharm™; 0.5-1.0 mg/kg) was applied subcutaneously for post-operative pain management. To reduce chances of rupture at the repair site, the FDL tendon was first transected at the myotendinous junction (MTJ) and the skin was closed with non-resorbable 5-0 suture (#668G Ethilon, Ethicon Inc., Bridgewater, NJ, USA). Transection of the MTJ results in a transient decrease in loading, with reintegration of the MTJ observed by day 7-10 post-surgery in this model. Following sterilization of the surgery site, a small incision was made on the plantar surface of the right hind paw. The FDL tendon was carefully

located, completely transected at the mid substance, and repaired using non-resorbable 8-0 suture (#2808G Ethilon, Ethicon Inc.) using a modified Kessler pattern. Skin over the surgery site was closed with 5-0 suture. Mice were carefully monitored for 72 hours post-surgery to ensure their return to prior cage activity, food intake, and water consumption.

Histology and immunofluorescence

Hind paws were harvested (n = 3-5 per timepoint) from uninjured GLAST^{Ai9} and GLAST^{Ai9}; Scx^{GFP} mice, and GLAST^{Ai9}; Scx^{GFP} at days 3, 7, 10, 14, 21, and 28 days post-injury for paraffin sectioning. Hind paws were fixed in 10% neutral buffered formalin (NBF) for 72 hours at room temperature, decalcified for two weeks, processed, and embedded in paraffin. Three-micron sagittal sections were cut, deparaffinized, and rehydrated. Antigen retrieval (10mM sodium citrate, 0.05% Tween-20, pH 6.0) was performed at 75°C for 4 hours. Slides were blocked in blocking buffer (10% normal donkey serum [NDS; #017-000-121, Jackson ImmunoResearch, West Grove, PA, USA] in PBS + 0.1% Tween-20 [PBST]) for 1 hour at room temperature. For non-conjugated mouse antibodies (*e.g.*, mouse anti-myosin) listed below, 30 µg/mL goat anti mouse IgG Fab fragment (#115-007-003, Jackson ImmunoResearch) was added to the blocking buffer. Slides were then incubated with antibodies to tdTomato (1:500, AB8181, SICGEN, Cantanhede, PT), GFP (1:500, ab290, Abcam, Cambridge, UK), myosin (1:50, ab37484, Abcam), alpha-smooth muscle actin (αSMA-FITC, 1:500, F3777, Sigma Alrich), CD146 (1:500, ab75769, Abcam), CCN3 (1:100, ab137677, Abcam), or Ki67 (1:250, ab16667, Abcam) in blocking buffer overnight at 4°C. The following secondary antibodies were used (all used at 1:200, all AffiniPure F(ab')$_2$ Fragment, Jackson ImmunoResearch): donkey anti-goat Rhodamine-Red-X (RRX) for tdTomato (#705-296-147), donkey anti-rabbit 488 for GFP and Ki67 (#711-546-152), donkey anti-rabbit RRX for CCN3 (#711- 296-152), and donkey anti-mouse 488 for myosin (#715-546-150). All secondary antibody incubations were performed for 1 hour at room temperature. Nuclei were counterstained with Hoechst 33342 (NucBlue™ Live ReadyProbes™ Reagent, Thermo Fisher Scientific, Waltham, MA, USA) and slides were cover slipped (ProLong™

Diamond Antifade Mountant, Thermo Fisher Scientific). Imaging was performed using a VS120 Virtual Slide Microscope (Olympus, Waltham, MA, USA) and images were pseudo-colored in OlyVIA (V3.3, Olympus) for ease of visualization and accessibility.

Quantification of cell populations during healing

Fluorescent images were quantified with VIS Image Analysis Software (v.6.7.0.2590, Visiopharm, Hørsholm, DK) as previously described.[65,66] Briefly, a region of interest (ROI) was drawn around the scar area (excluding tendon stubs). Individual nuclei were then identified by automatic segmentation and were subsequently assigned a specific identity based on intensity thresholds of each color channel. The total number of cells was determined based on the number of nuclei identified, and the percentage of each cell population is given as a percentage of this total cell number. An n = 2-5 repairs was used for quantification of cell populations (GLAST^{Ai9}, GLAST^{Ai9}; Scx^{GFP}, Scx^{GFP}, or double negative) as well as proliferating GLAST^{Ai9} (GLAST^{Ai9}; Ki67+) during tendon healing.

Human tissue histology

Normal human tendon tissue from uninjured flexor tendons (n= 2) was obtained after informed consent and was approved by the Research Subjects Review Board at the University of Rochester (protocol #54231). In addition, peritendinous scar tissue was obtained from patients (n= 3) undergoing tenolysis procedure. All human samples were processed for routine paraffin histology. Three-micron sagittal sections were cut, deparaffinized, rehydrated, probed with antibodies to GLAST (EAAT1, 1:250, ab416, Abcam) or CCN3 as described above, and visualized using a donkey-anti rabbit RRX secondary antibody. Imaging and pseudo-coloring were performed as described above.

Second harmonic generation two-photon microscopy

To visualize the relationship between GLAST^{Ai9} cells and the tendon collagen matrix using second harmonic generation (SHG) imaging, uninjured hind paws from GLAST^{Ai9} mice (n=3) were harvested

for frozen sectioning as previously described.[20,65] Briefly, hind paws were fixed for 24 hours in 10% NBF, decalcified for 5 days in EDTA, and incubated in 30% sucrose for 24 hours to cryo-protect the tissue. 20μm sagittal and axial sections of intact FDL tendons were cut using a cryotape-transfer method[67] and nuclei were stained with Hoechst 33342 as described above. Z-stack images of endogenous tdTomato expression in GLAST^{Ai9} cells along with the collagen SHG of the tendon body were then acquired in the URMC Multiphoton and Analytical Imaging Center (MAGIC) Core using an Olympus FVMPE-RS system and tunable Insight X3 laser. Images were pseudo-colored and analyzed in Fiji (https://fiji.sc/).[68] 3D projections and renderings of image stacks were generated using the 3D Project function and 3D Viewer plugin, respectively.

In situ two-photon microscopy

Hind paws from GLAST^{Ai9} mice were harvested 14 days following the final TMX injection. The skin on the plantar surface of the hind paw was removed, and the superficial-most muscle on the bottom of the hind paw was carefully dissected and removed to expose the FDL tendon. Dissected hind paws were then fixed for 24 hours in 10% NBF at 4°C, protected from light. To visualize the location of GLAST^{Ai9} cells relative to blood vessels on the surface of the tendon, hind paws were stained with antibodies to αSMA which labels vascular smooth muscle cells. Following fixation, hind paws were rinsed, blocked (blocking buffer, 1 hour at room temperature), and incubated with conjugated antibodies to αSMA (αSMA-FITC, 1:500, F3777, Sigma Aldrich) in blocking buffer for 48 hours at 4°C, protected from light. Hind paws were rinsed again, and nuclei were counterstained with Hoechst 33342 for 1 hour at room temperature. For imaging, hind paws were anchored plantar side up in a clear putty (Crazy Aaron's Thinking Putty®, Liquid Glass®, Crazy Aaron Enterprises, Norristown, PA, USA) and covered with PBS. Z-stack images of the epitenon were acquired in the URMC MAGIC Core and images were analyzed and pseudocolored in Fiji as described above. 3D projections and renderings of image stacks were generated using the 3D Project function and 3D Viewer plugin, respectively.

Single cell isolation

Mouse

In order to isolate sufficient cells for single cell RNA-sequencing (scRNA-seq), tendons from individual GLAST^{Ai9} mice were pooled for isolation (12x intact tendons, 5x day 7 repairs, 3x day 14 repairs, and 3x day 28 repairs). Intact tendons were harvested from the heel to just proximal to the digit bifurcation. For injured tendons, the entire scar area was carefully dissected away from surrounding tissue and the scar along with approximately 1 mm of tendon stub on either side of the repair was harvested. Tendons were placed into low glucose (1 g/L) Dulbecco's Modified Eagle Medium (DMEM; 11885084, Gibco, Thermo Fisher Scientific) on ice, and digested in DMEM containing Collagenase Type I (LS004196, Worthington Biochemical, Lakewood, NJ, USA) and Collagenase Type IV (LS004188, Worthington Biochemical) at a final concentration of 5 mg/ml and 1 mg/ml, respectively. Samples were digested at 37°C with rotation for approximately 2 hours for intact tendons and 45 minutes for injured tendons. This protocol was optimized to ensure high quality cells for sequencing. After digestion, the cell suspension was sequentially filtered through 70 µm and 50 µm cell strainers to remove any debris, pelleted at 500xg for 10 minutes at 4°C, rinsed twice in Dulbecco's Phosphate Buffer Solution (dPBS; 14190136, Gibco), and finally resuspended in 0.5% Bovine Serum Albumin (BSA; Fraction V, 10735078001, Roche, Basel, CH) in dPBS at a concentration of 1,200 cells/µL.

Human

Peritendinous scar tissue was obtained from a single individual (34-year-old male with lacerations to his flexor pollicis longus and all flexor digitorum profundus/ superficialis tendons) with approval by the Research Subjects Review Board at the University of Rochester (protocol #54231). Eight months following initial repair, the patient underwent a tenolysis procedure to restore digit range of motion. Peritendinous scar tissue was removed during surgery, harvested into low glucose DMEM on ice, and immediately processed for scRNA-seq. Fatty tissue was removed and fibrous scar tissue was minced into small (~1mm) pieces before being digested in DMEM containing Collagenase Type I

and Type IV as described above. Tissue was incubated at 37°C for approximately 1 hour until completely digested before being filtered, rinsed, and resuspended in 0.5% as described above.

Single cell RNA-sequencing

For both species, libraries were prepared and sequenced by the UR Genomics Research Center (GRC). 10,000 cells per sample were loaded into Chromium Controller (10X Genomics, Pleasanton, CA, USA) for single-cell capture. Libraries were then prepared using the Chromium Single Cell 3' Reagent Kit v3 (#1000075, 10X Genomics). Following library preparation and quality control (QC), libraries were sequenced using the S2 NovaSeq flow cell system (Illumina, San Diego, CA) generating an average of 1.7×10^9 billion reads per sample (~140,000 reads per cell) for mouse and 7.6×10^6 reads (~105,446 per cell) for human. Reads were processed using CellRanger (v6.0.1,10X Genomics) and aligned to either the human reference genome (GRCh38-2020-A) or a modified version of the mouse genome (GRCm38/mm10) containing the mRNA sequence for *tdTomato* from the *ROSA-Ai9* targeting vector (#22799, Addgene, Watertown, MA, USA) to facilitate identification of $GLAST^{Ai9}$ cells in the scRNA-seq datasets.

Mouse healing single cell RNA-seq data processing, annotation, and integration

All scRNA-seq analysis was performed using RStudio (v1.4.1717). Datasets from each timepoint were processed individually using the Seurat R package (v4.3.0).[69] Low quality cells with low feature numbers or mitochondrial gene content greater than 5% were excluded from the dataset, resulting in a total of 6,320 cells for the uninjured sample, 4,470 for the day 7 samples, 4,841 for the day 14 sample, and 4,609 cells for the day 28 sample. Read data for each sample was normalized (normalization.method = "LogNormalize", scale.factor = 10000) and the top 2000 most variable features were identified (selection.method = "vst") for use in downstream analysis. Data was scaled, and dimensionality reduction was performed by *RunPCA* using the highly variable features with default parameters. Unsupervised clustering was then performed using the *FindNeighbors* function to

compute the shared nearest-neighbors (SNN) for each sample (dims = 1:20) and the *FindClusters* function (resolution = 0.1). Clusters were visualized as Uniform Manifold Approximation and Projection (UMAP) plots in two dimensions. Differentially expressed genes (DEGs) for each cluster were identified using the *FindAllMarkers* function (min.pct = 0.25, logfc.threshold = 0.25). To aid in annotating individual clusters, gene ontology (GO) enrichment analysis was performed with the DAVID Gene Functional Classification Tool (http://david.abcc.ncifcrf.gov; version 6.8)[70] using the top 100 DEG from each cluster. To trace the fate of GLAST^{Ai9} epitenon cells throughout healing, the uninjured dataset was integrated with datasets from days 7, 14, and 28 post-injury using the *FindIntegrationAnchors* and *IntegrateData* functions (dims = 1:20). Scaled data was used for PCA (npcs = 30) and UMAP dimensional reduction. Cell clusters were visualized (resolution = 0.21) and identified as described above. For both the individual timepoints and the integrated dataset, GLAST^{Ai9} cells were identified as any cell with normalized *tdTomato* expression >0.05. Similarly, Scx+ cells were identified as any cell with normalized *Scx* expression >0.3.

Pseudotime and transcription factor enrichment analysis

The tenogenic and pro-fibrotic differentiation trajectories of epitenon cells during healing were modeled using the Monocle3 R package (v.3.1.2.9).[71,72] Epitenon clusters (uninjured, day 7, and day 14) and epitenon-derived tenocyte (EDT) clusters (day 7, day 14, and day 28) were subset from the integrated dataset and converted into a Monocle3 object using the SeuratWrappers R package (v0.3.1). As the EDT cluster appears post-injury, no uninjured EDT cells were able to be included in the trajectory analysis. The day 28 epitenon cell cluster was excluded from the pseudotime analysis as cells at this timepoint appear to be reverting back to the uninjured epitenon phenotype (**Fig. S5B**) and therefore were not representative of the pro-fibrotic phenotype of interest. Cells were re-clustered (resolution = 0.001) and the functions *learn_graph* and *order_cells* were utilized to order cells in pseudotime and to identify potential differentiation trajectories using the uninjured epitenon cell cluster as the root. The *graph_test* and *find_gene_modules* (resolution = 0.001, k = 13) functions

were then used to generate gene modules (groups of genes that vary over pseudotime) by hierarchical cluster analysis. GO enrichment analysis was subsequently performed to determine enriched biological processes in each module. To determine potential transcription factors (TF) that may be involved in regulating either the tenogenic or pro-fibrotic fate of epitenon cells post-injury, transcription factor enrichment analysis was performed using the web-based ChEA3 tool (https://maayanlab.cloud/chea3/).[73] For each module, the top 5 transcription factors were selected and plotted over pseudotime using the *plot_genes_in_pseudotime* function.

Human and mouse scRNA-seq integration

The processed and annotated human peritendinous scar and mouse healing scRNA-seq datasets described above were integrated using NicheNet (v1.1.1)[74] and the reference mapping function in the Seurat R package. First, human gene symbols were converted to mouse symbols using *convert_human_to_mouse_symbols* function in NicheNet, retaining only human genes with one-to-one mouse orthologs. Human cells were then mapped to their corresponding mouse clusters using the Seurat function *FindTransferAnchors* (reference = mouse UMAP, query = human UMAP, dims = 1:20, reference.reduction = “pca”).

REFERENCES

1. Nichols, A.E.C., Best, K.T., and Loiselle, A.E. (2019). The cellular basis of fibrotic tendon healing: challenges and opportunities. Translational Research *209*, 156-168. 10.1016/j.trsl.2019.02.002.
2. Pennisi, E. (2002). Tending tender tendons. Science (New York, N.Y.) *295*, 1011. 10.1126/science.295.5557.1011.
3. Mehrzad, R., Mookerjee, V., Schmidt, S., Jehle, C.C., Kiwanuka, E., and Liu, P.Y. (2019). The Economic Impact of Flexor Tendon Lacerations of the Hand in the United States. Ann Plast Surg *83*, 419-423. 10.1097/sap.0000000000001950.
4. Strickland, J.W., and Glogovac, S.V. (1980). Digital function following flexor tendon repair in Zone II: A comparison of immobilization and controlled passive motion techniques. J Hand Surg Am *5*, 537-543. 10.1016/s0363-5023(80)80101-8.
5. Quadlbauer, S., Pezzei, C., Jurkowitsch, J., Reb, P., Beer, T., and Leixnering, M. (2016). Early Passive Movement in flexor tendon injuries of the hand. Archives of orthopaedic and traumatic surgery. Archiv fur orthopadische und Unfall-Chirurgie *136*, 285-293. 10.1007/s00402-015-2362-z.
6. Civan, O., Gürsoy, M.K., Cavit, A., Özcanlı, H., and Karalezli, M.N. (2020). Tenolysis rate after zone 2 flexor tendon repairs. Jt Dis Relat Surg *31*, 281-285. 10.5606/ehc.2020.71752.
7. Garner, W.L., McDonald, J.A., Koo, M., Kuhn, C., 3rd, and Weeks, P.M. (1989). Identification of the collagen-producing cells in healing flexor tendons. Plastic and reconstructive surgery *83*, 875-879. 10.1097/00006534-198905000-00018.
8. Gelberman, R.H., Steinberg, D., Amiel, D., and Akeson, W. (1991). Fibroblast chemotaxis after tendon repair. J Hand Surg Am *16*, 686-693. 10.1016/0363-5023(91)90195-h.
9. Gelberman, R.H., Vandeberg, J.S., Manske, P.R., and Akeson, W.H. (1985). The early stages of flexor tendon healing: a morphologic study of the first fourteen days. J Hand Surg Am *10*, 776-784. 10.1016/s0363-5023(85)80151-9.

10. Manske, P.R., Lesker, P.A., Gelberman, R.H., and Rucinsky, T.E. (1985). Intrinsic restoration of the flexor tendon surface in the nonhuman primate. J Hand Surg Am *10*, 632-637. 10.1016/s0363-5023(85)80198-2.

11. Khan, U., Edwards, J.C., and McGrouther, D.A. (1996). Patterns of cellular activation after tendon injury. J Hand Surg Br *21*, 813-820. 10.1016/s0266-7681(96)80199-9.

12. Mori, T., Tanaka, K., Buffo, A., Wurst, W., Kühn, R., and Götz, M. (2006). Inducible gene deletion in astroglia and radial glia--a valuable tool for functional and lineage analysis. Glia *54*, 21-34. 10.1002/glia.20350.

13. Kan, L., Peng, C.Y., McGuire, T.L., and Kessler, J.A. (2013). Glast-expressing progenitor cells contribute to heterotopic ossification. Bone *53*, 194-203. 10.1016/j.bone.2012.12.008.

14. Kan, C., Ding, N., Yang, J., Tan, Z., McGuire, T.L., Lu, H., Zhang, K., Berger, D.M.P., Kessler, J.A., and Kan, L. (2019). BMP-dependent, injury-induced stem cell niche as a mechanism of heterotopic ossification. Stem Cell Research & Therapy *10*, 14. 10.1186/s13287-018-1107-7.

15. Göritz, C., Dias, D.O., Tomilin, N., Barbacid, M., Shupliakov, O., and Frisén, J. (2011). A pericyte origin of spinal cord scar tissue. Science (New York, N.Y.) *333*, 238-242. 10.1126/science.1203165.

16. Madisen, L., Zwingman, T.A., Sunkin, S.M., Oh, S.W., Zariwala, H.A., Gu, H., Ng, L.L., Palmiter, R.D., Hawrylycz, M.J., Jones, A.R., et al. (2010). A robust and high-throughput Cre reporting and characterization system for the whole mouse brain. Nat Neurosci *13*, 133-140. 10.1038/nn.2467.

17. Kannus, P. (2000). Structure of the tendon connective tissue. Scandinavian journal of medicine & science in sports *10*, 312-320.

18. Yang, S.M., Alvarez, D.D., and Schinder, A.F. (2015). Reliable Genetic Labeling of Adult-Born Dentate Granule Cells Using Ascl1^{CreERT2} and Glast^{CreERT2} Murine Lines. The Journal of Neuroscience *35*, 15379-15390. 10.1523/jneurosci.2345-15.2015.

19. Pryce, B.A., Brent, A.E., Murchison, N.D., Tabin, C.J., and Schweitzer, R. (2007). Generation of transgenic tendon reporters, ScxGFP and ScxAP, using regulatory elements of the scleraxis gene. Dev. Dyn.

20. Best, K.T., and Loiselle, A.E. (2019). Scleraxis lineage cells contribute to organized bridging tissue during tendon healing and identify a subpopulation of resident tendon cells. FASEB journal : official publication of the Federation of American Societies for Experimental Biology *33*, 8578-8587. 10.1096/fj.201900130RR.

21. Muhl, L., Genové, G., Leptidis, S., Liu, J., He, L., Mocci, G., Sun, Y., Gustafsson, S., Buyandelger, B., Chivukula, I.V., et al. (2020). Single-cell analysis uncovers fibroblast heterogeneity and criteria for fibroblast and mural cell identification and discrimination. Nature Communications *11*, 3953. 10.1038/s41467-020-17740-1.

22. Ackerman, J.E., Best, K.T., Muscat, S.N., Pritchett, E.M., Nichols, A.E.C., Wu, C.-L., and Loiselle, A.E. (2022). Defining the spatial-molecular map of fibrotic tendon healing and the drivers of Scleraxis-lineage cell fate and function. Cell Reports *41*, 111706. https://doi.org/10.1016/j.celrep.2022.111706.

23. Best, K.T., Korcari, A., Mora, K.E., Nichols, A.E., Muscat, S.N., Knapp, E., Buckley, M.R., and Loiselle, A.E. (2021). Scleraxis-lineage cell depletion improves tendon healing and disrupts adult tendon homeostasis. eLife *10*. 10.7554/eLife.62203.

24. Korcari, A., Muscat, S., McGinn, E., Buckley, M.R., and Loiselle, A.E. (2022). Depletion of Scleraxis-lineage cells during tendon healing transiently impairs multi-scale restoration of tendon structure during early healing. PloS one *17*, e0274227. 10.1371/journal.pone.0274227.

25. Lee, C.H., Lee, F.Y., Tarafder, S., Kao, K., Jun, Y., Yang, G., and Mao, J.J. (2015). Harnessing endogenous stem/progenitor cells for tendon regeneration. Journal of Clinical Investigation *125*, 2690-2701. 10.1172/jci81589.

26. Bi, Y., Ehirchiou, D., Kilts, T.M., Inkson, C.A., Embree, M.C., Sonoyama, W., Li, L., Leet, A.I., Seo, B.M., Zhang, L., et al. (2007). Identification of tendon stem/progenitor cells and the role of the extracellular matrix in their niche. Nature medicine *13*, 1219-1227. 10.1038/nm1630.

27. Dyment, N.A., Liu, C.-F., Kazemi, N., Aschbacher-Smith, L.E., Kenter, K., Breidenbach, A.P., Shearn, J.T., Wylie, C., Rowe, D.W., and Butler, D.L. (2013). The Paratenon Contributes to Scleraxis-Expressing Cells during Patellar Tendon Healing. PloS one.

28. Dahlgren, L.A., van der Meulen, M.C., Bertram, J.E., Starrak, G.S., and Nixon, A.J. (2002). Insulin-like growth factor-I improves cellular and molecular aspects of healing in a collagenase-induced model of flexor tendinitis. Journal of orthopaedic research : official publication of the Orthopaedic Research Society *20*, 910-919. 10.1016/s0736-0266(02)00009-8.

29. Kurtz, C.A., Loebig, T.G., Anderson, D.D., DeMeo, P.J., and Campbell, P.G. (1999). Insulin-like growth factor I accelerates functional recovery from Achilles tendon injury in a rat model. The American journal of sports medicine *27*, 363-369. 10.1177/03635465990270031701.

30. Provenzano, P.P., Alejandro-Osorio, A.L., Grorud, K.W., Martinez, D.A., Vailas, A.C., Grindeland, R.E., and Vanderby, R., Jr. (2007). Systemic administration of IGF-I enhances healing in collagenous extracellular matrices: evaluation of loaded and unloaded ligaments. BMC Physiol *7*, 2. 10.1186/1472-6793-7-2.

31. Tsogtbaatar, E., Landin, C., Minter-Dykhouse, K., and Folmes, C.D.L. (2020). Energy Metabolism Regulates Stem Cell Pluripotency. Frontiers in Cell and Developmental Biology *8*. 10.3389/fcell.2020.00087.

32. Ito, Y., Toriuchi, N., Yoshitaka, T., Ueno-Kudoh, H., Sato, T., Yokoyama, S., Nishida, K., Akimoto, T., Takahashi, M., Miyaki, S., and Asahara, H. (2010). The Mohawk homeobox gene is a critical regulator of tendon differentiation. Proc. Natl. Acad. Sci. U.S.A.

33. Harvey, T., Flamenco, S., and Fan, C.-M. (2019). A Tppp3+Pdgfra+ tendon stem cell population contributes to regeneration and reveals a shared role for PDGF signalling in regeneration and fibrosis. Nature cell biology *21*, 1490-1503. 10.1038/s41556-019-0417-z.

34. Wang, Y., Zhang, X., Huang, H., Xia, Y., Yao, Y., Mak, A.F.-T., Yung, P.S.-H., Chan, K.-M., Wang, L., Zhang, C., et al. (2017). Osteocalcin expressing cells from tendon sheaths in mice contribute to tendon repair by activating Hedgehog signaling. eLife *6*, e30474. 10.7554/eLife.30474.

35. Grinstein, M., Tsai, S.L., Montoro, D., Dingwall, H.L., Zou, K., Sade-Feldman, M., Tanaka, M.J., Capellini, T.D., Rajagopal, J., and Galloway, J.L. (2022). A quiescent resident progenitor pool is the central organizer of tendon healing. bioRxiv, 2022.2002.2002.478533. 10.1101/2022.02.02.478533.

36. Walia, B., Li, T.M., Crosio, G., Montero, A.M., and Huang, A.H. (2022). Axin2-lineage cells contribute to neonatal tendon regeneration. Connective tissue research *63*, 530-543. 10.1080/03008207.2022.2036732.

37. Howell, K., Chien, C., Bell, R., Laudier, D., Tufa, S.F., Keene, D.R., Andarawis-Puri, N., and Huang, A.H. (2017). Novel Model of Tendon Regeneration Reveals Distinct Cell Mechanisms Underlying Regenerative and Fibrotic Tendon Healing. Scientific reports *7*, 45238. 10.1038/srep45238.

38. De Micheli, A.J., Swanson, J.B., Disser, N.P., Martinez, L.M., Walker, N.R., Oliver, D.J., Cosgrove, B.D., and Mendias, C.L. (2020). Single-cell transcriptomic analysis identifies extensive heterogeneity in the cellular composition of mouse Achilles tendons. American journal of physiology. Cell physiology *319*, C885-c894. 10.1152/ajpcell.00372.2020.

39. Huang, A.H., Lu, H.H., and Schweitzer, R. (2015). Molecular regulation of tendon cell fate during development. Journal of orthopaedic research : official publication of the Orthopaedic Research Society *33*, 800-812. 10.1002/jor.22834.

40. Kaji, D.A., Montero, A.M., Patel, R., and Huang, A.H. (2021). Transcriptional profiling of mESC-derived tendon and fibrocartilage cell fate switch. Nat Commun *12*, 4208. 10.1038/s41467-021-24535-5.

41. Schweitzer, R., Chyung, J.H., Murtaugh, L.C., Brent, A.E., Rosen, V., Olson, E.N., Lassar, A., and Tabin, C.J. (2001). Analysis of the tendon cell fate using Scleraxis, a specific marker for tendons and ligaments. Development (Cambridge, England).

42. Cserjesi, P., Brown, D., Ligon, K.L., Lyons, G.E., Copeland, N.G., Gilbert, D.J., Jenkins, N.A., and Olson, E.N. (1995). Scleraxis: a basic helix-loop-helix protein that prefigures skeletal formation during mouse embryogenesis. Development (Cambridge, England).

43. Ith, B., Wei, J., Yet, S.-F., Perrella, M.A., and Layne, M.D. (2005). Aortic carboxypeptidase-like protein is expressed in collagen-rich tissues during mouse embryonic development. Gene Expression Patterns *5*, 533-537. https://doi.org/10.1016/j.modgep.2004.11.002.

44. Leussink, B., Brouwer, A., el Khattabi, M., Poelmann, R.E., Gittenberger-de Groot, A.C., and Meijlink, F. (1995). Expression patterns of the paired-related homeobox genes MHox/Prx1 and S8/Prx2 suggest roles in development of the heart and the forebrain. Mech Dev *52*, 51-64. 10.1016/0925-4773(95)00389-i.

45. Stricker, S., Mathia, S., Haupt, J., Seemann, P., Meier, J., and Mundlos, S. (2012). Odd-skipped related genes regulate differentiation of embryonic limb mesenchyme and bone marrow mesenchymal stromal cells. Stem cells and development *21*, 623-633. 10.1089/scd.2011.0154.

46. Chanda, D., Kurundkar, A., Rangarajan, S., Locy, M., Bernard, K., Sharma, N.S., Logsdon, N.J., Liu, H., Crossman, D.K., Horowitz, J.C., et al. (2016). Developmental Reprogramming in Mesenchymal Stromal Cells of Human Subjects with Idiopathic Pulmonary Fibrosis. Scientific reports *6*, 37445. 10.1038/srep37445.

47. Valcourt, U., Thuault, S., Pardali, K., Heldin, C.H., and Moustakas, A. (2007). Functional role of Meox2 during the epithelial cytostatic response to TGF-beta. Mol Oncol *1*, 55-71. 10.1016/j.molonc.2007.02.002.

48. Alexanian, M., Przytycki, P.F., Micheletti, R., Padmanabhan, A., Ye, L., Travers, J.G., Gonzalez-Teran, B., Silva, A.C., Duan, Q., Ranade, S.S., et al. (2021). A transcriptional switch

governs fibroblast activation in heart disease. Nature *595*, 438-443. 10.1038/s41586-021-03674-1.

49. Chen, Y., Rabson, A.B., and Gorski, D.H. (2010). MEOX2 regulates nuclear factor-kappaB activity in vascular endothelial cells through interactions with p65 and IkappaBbeta. Cardiovasc Res *87*, 723-731. 10.1093/cvr/cvq117.

50. Best, K.T., Lee, F.K., Knapp, E., Awad, H.A., and Loiselle, A.E. (2019). Deletion of NFKB1 enhances canonical NF-κB signaling and increases macrophage and myofibroblast content during tendon healing. Scientific reports *9*, 10926. 10.1038/s41598-019-47461-5.

51. Best, K.T., Nichols, A.E.C., Knapp, E., Hammert, W.C., Ketonis, C., Jonason, J.H., Awad, H.A., and Loiselle, A.E. (2020). NF-κB activation persists into the remodeling phase of tendon healing and promotes myofibroblast survival. Sci Signal *13*. 10.1126/scisignal.abb7209.

52. Ramachandran, A., Gong, E.M., Pelton, K., Ranpura, S.A., Mulone, M., Seth, A., Gomez, P., 3rd, and Adam, R.M. (2011). FosB regulates stretch-induced expression of extracellular matrix proteins in smooth muscle. The American Journal of Pathology *179*, 2977-2989. 10.1016/j.ajpath.2011.08.034.

53. Morita, W., Snelling, S.J., Dakin, S.G., and Carr, A.J. (2016). Profibrotic mediators in tendon disease: a systematic review. Arthritis Research & Therapy *18*, 269. 10.1186/s13075-016-1165-0.

54. Chiquet-Ehrismann, R., and Chiquet, M. (2003). Tenascins: regulation and putative functions during pathological stress. The Journal of pathology *200*, 488-499. 10.1002/path.1415.

55. Riley, G. (2008). Tendinopathy--from basic science to treatment. Nature clinical practice. Rheumatology *4*, 82-89. 10.1038/ncprheum0700.

56. Downes, M., and Koopman, P. (2001). SOX18 and the transcriptional regulation of blood vessel development. Trends Cardiovasc Med *11*, 318-324. 10.1016/s1050-1738(01)00131-1.

57. Olbromski, M., Podhorska-Okołów, M., and Dzięgiel, P. (2018). Role of the SOX18 protein in neoplastic processes. Oncol Lett *16*, 1383-1389. 10.3892/ol.2018.8819.

58. Kawai, S., Yamauchi, M., Wakisaka, S., Ooshima, T., and Amano, A. (2007). Zinc-finger transcription factor odd-skipped related 2 is one of the regulators in osteoblast proliferation and bone formation. J Bone Miner Res *22*, 1362-1372. 10.1359/jbmr.070602.

59. Kendal, A.R., Layton, T., Al-Mossawi, H., Appleton, L., Dakin, S., Brown, R., Loizou, C., Rogers, M., Sharp, R., and Carr, A. (2020). Multi-omic single cell analysis resolves novel stromal cell populations in healthy and diseased human tendon. Scientific reports *10*, 13939. 10.1038/s41598-020-70786-5.

60. Akbar, M., MacDonald, L., Crowe, L.A.N., Carlberg, K., Kurowska-Stolarska, M., Ståhl, P.L., Snelling, S.J.B., McInnes, I.B., and Millar, N.L. (2021). Single cell and spatial transcriptomics in human tendon disease indicate dysregulated immune homeostasis. Ann Rheum Dis *80*, 1494-1497. 10.1136/annrheumdis-2021-220256.

61. Still, C., Chang, W.-T., Sherman, S.L., Sochacki, K.R., Dragoo, J.L., and Qi, L.S. (2021). Single-cell transcriptomic profiling reveals distinct mechanical responses between normal and diseased tendon progenitor cells. Cell Reports Medicine *2*, 100343. https://doi.org/10.1016/j.xcrm.2021.100343.

62. Pryce, B.A., Brent, A.E., Murchison, N.D., Tabin, C.J., and Schweitzer, R. (2007). Generation of transgenic tendon reporters, ScxGFP and ScxAP, using regulatory elements of the scleraxis gene. Developmental dynamics : an official publication of the American Association of Anatomists *236*, 1677-1682. 10.1002/dvdy.21179.

63. Ackerman, J.E., and Loiselle, A.E. (2016). Murine Flexor Tendon Injury and Repair Surgery. Journal of visualized experiments : JoVE. 10.3791/54433.

64. Best, K.T., Mora, K.E., Knapp, E., Buckley, M.R., and Loiselle, A.E. (2020). Scleraxis-Lineage Cell Depletion Improves Tendon Healing. bioRxiv.

65. Muscat, S., Nichols, A.E.C., Gira, E., and Loiselle, A.E. (2022). CCR2 is expressed by tendon resident macrophage and T cells, while CCR2 deficiency impairs tendon healing via blunted

involvement of tendon-resident and circulating monocytes/macrophages. The FASEB Journal *36*, e22607. https://doi.org/10.1096/fj.202201162R.

66. Nichols, A.E.C., Muscat, S.N., Miller, S.E., Green, L.J., Richards, M.S., and Loiselle, A.E. (2021). Impact of isolation method on cellular activation and presence of specific tendon cell subpopulations during in vitro culture. FASEB journal : official publication of the Federation of American Societies for Experimental Biology *35*, e21733. 10.1096/fj.202100405R.

67. Dyment, N.A., Jiang, X., Chen, L., Hong, S.H., Adams, D.J., Ackert-Bicknell, C., Shin, D.G., and Rowe, D.W. (2016). High-Throughput, Multi-Image Cryohistology of Mineralized Tissues. Journal of visualized experiments : JoVE. 10.3791/54468.

68. Schindelin, J., Arganda-Carreras, I., Frise, E., Kaynig, V., Longair, M., Pietzsch, T., Preibisch, S., Rueden, C., Saalfeld, S., Schmid, B., et al. (2012). Fiji: an open-source platform for biological-image analysis. Nature methods *9*, 676-682. 10.1038/nmeth.2019.

69. Hao, Y., Hao, S., Andersen-Nissen, E., Mauck, W.M., Zheng, S., Butler, A., Lee, M.J., Wilk, A.J., Darby, C., Zager, M., et al. (2021). Integrated analysis of multimodal single-cell data. Cell *184*, 3573-3587.e3529. https://doi.org/10.1016/j.cell.2021.04.048.

70. Huang, D.W., Sherman, B.T., Tan, Q., Collins, J.R., Alvord, W.G., Roayaei, J., Stephens, R., Baseler, M.W., Lane, H.C., and Lempicki, R.A. (2007). The DAVID Gene Functional Classification Tool: a novel biological module-centric algorithm to functionally analyze large gene lists. Genome biology *8*, R183. 10.1186/gb-2007-8-9-r183.

71. Trapnell, C., Cacchiarelli, D., Grimsby, J., Pokharel, P., Li, S., Morse, M., Lennon, N.J., Livak, K.J., Mikkelsen, T.S., and Rinn, J.L. (2014). The dynamics and regulators of cell fate decisions are revealed by pseudotemporal ordering of single cells. Nature Biotechnology *32*, 381-386. 10.1038/nbt.2859.

72. Qiu, X., Mao, Q., Tang, Y., Wang, L., Chawla, R., Pliner, H.A., and Trapnell, C. (2017). Reversed graph embedding resolves complex single-cell trajectories. Nature methods *14*, 979-982. 10.1038/nmeth.4402.

73. Keenan, A.B., Torre, D., Lachmann, A., Leong, A.K., Wojciechowicz, M.L., Utti, V., Jagodnik, K.M., Kropiwnicki, E., Wang, Z., and Ma'ayan, A. (2019). ChEA3: transcription factor enrichment analysis by orthogonal omics integration. Nucleic acids research *47*, W212-w224. 10.1093/nar/gkz446.

74. Browaeys, R., Saelens, W., and Saeys, Y. (2020). NicheNet: modeling intercellular communication by linking ligands to target genes. Nature methods *17*, 159-162. 10.1038/s41592-019-0667-5.

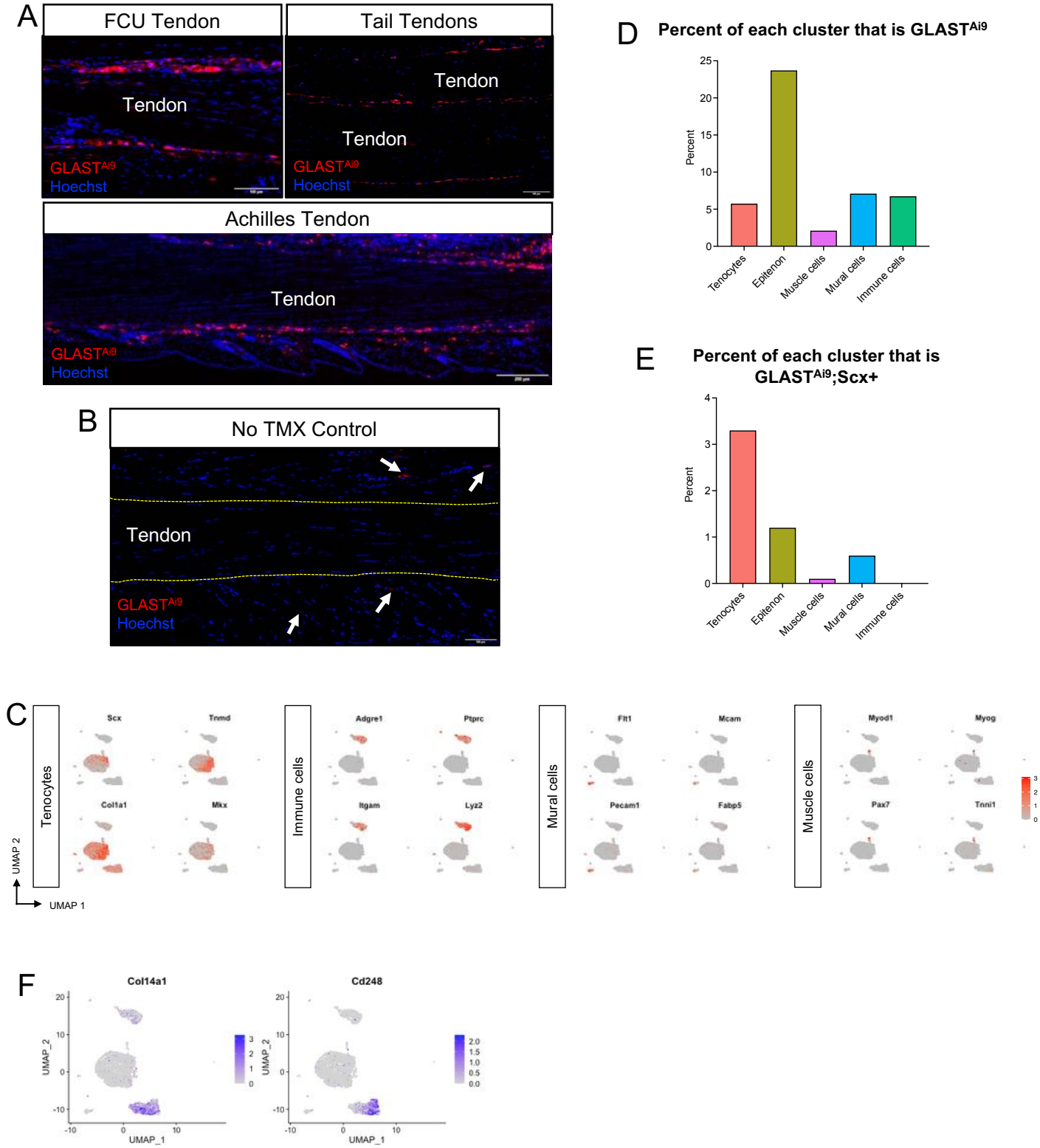

Fig. 1 supplement: (**A**) Representative images demonstrating GLAST^{Ai9} labeled epitenon cells (red) in the flexor carpi ulnaris (FCU), tail, and Achilles tendons of adult mice. (**B**) Representative image demonstrating lack of epitenon cell labeling in GLAST^{Ai9} mice without tamoxifen. The flexor digitorum longus (FDL) tendon is outline by yellow dotted lines. Some red cells were observed in surrounding tissues (ie. muscle; red cells, white arrows). (**C**) UMAP plots of markers used to annotate cell clusters in the uninjured scRNA-seq dataset. Quantification of the percentage of each cluster in the uninjured scRNA-seq dataset that was (**D**) GLAST^{Ai9} or (**E**) GLAST^{Ai9};Scx+. (**F**) UMAP plots of additional epitenon-specific transcriptional markers *Col14a1* and *Cd248*.

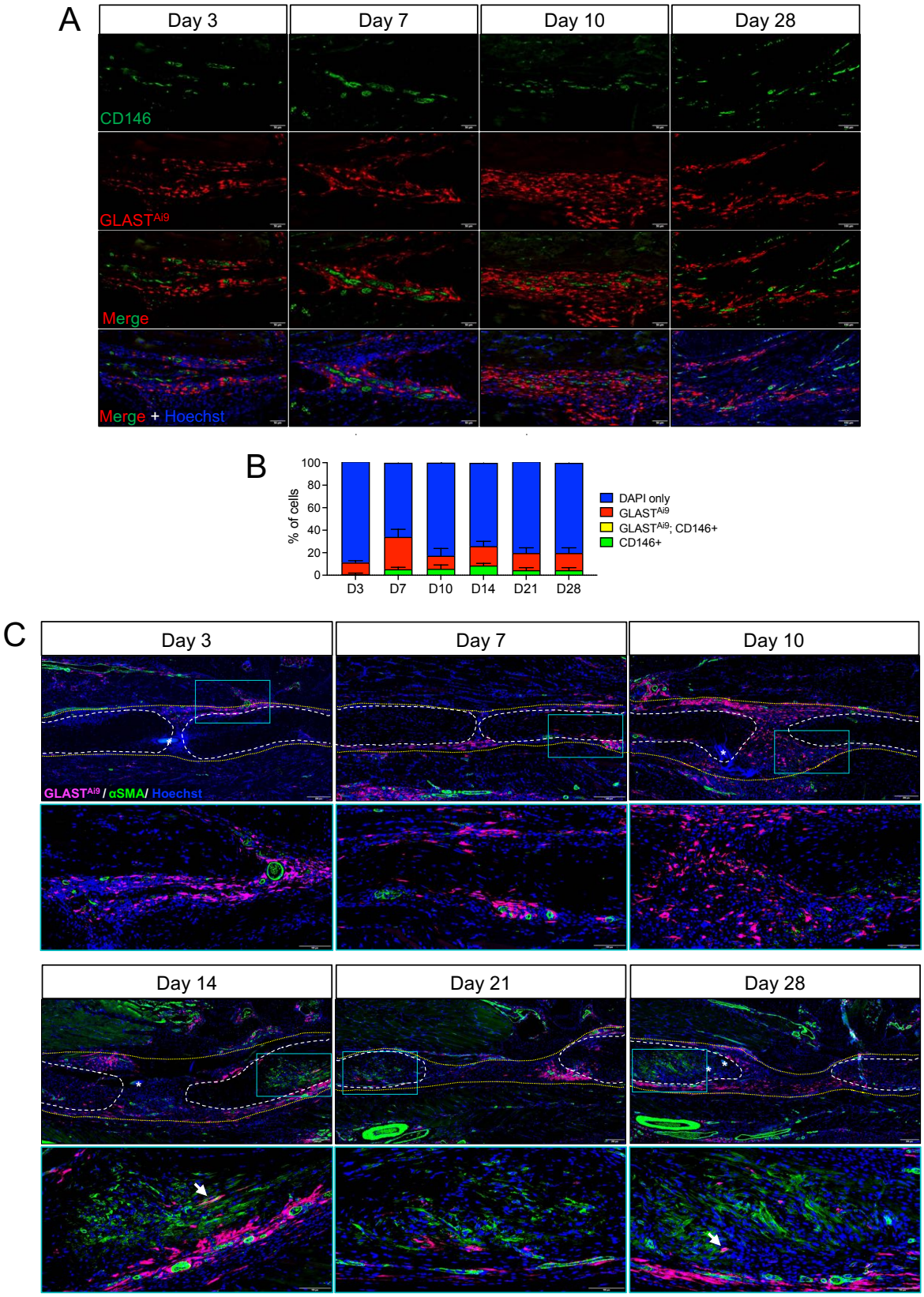

Fig. 3 supplement: (**A**) Representative images of healing tendons from GLAST^{Ai9}; Scx^{GFP} mice at 3, 7, 10, and 28 days post-injury demonstrating staining for CD146 (green) and GLAST^{Ai9} (red) cells in the scar area. No GLAST^{Ai9}; CD146+ cells were observed in any sample. Scale bars = 50 μm. (**B**) Quantification of GLAST^{Ai9} (red), CD146+ (green), GLAST^{Ai9};CD146+ cells (yellow), or double negative cells (blue) in the scar area throughout healing. (**C**) Representative images of healing tendons from GLAST^{Ai9}; Scx^{GFP} mice at 3, 7, 10, 14, 21, and 28 days post-injury stained for alpha smooth muscle actin (αSMA)+ myofibroblasts (green) and GLAST^{Ai9} (magenta) cells. White arrows denote GLAST^{Ai9} αSMA+ myofibroblasts in the tendon stubs. No GLAST^{Ai9} αSMA+ were found in the scar area. Scale bars = 200 μm (top), 100 μm (bottom). Sutures are marked by white asterisks. All images are representative of n = 2-4 mice. In all images, nuclei are counterstained with Hoechst (blue).

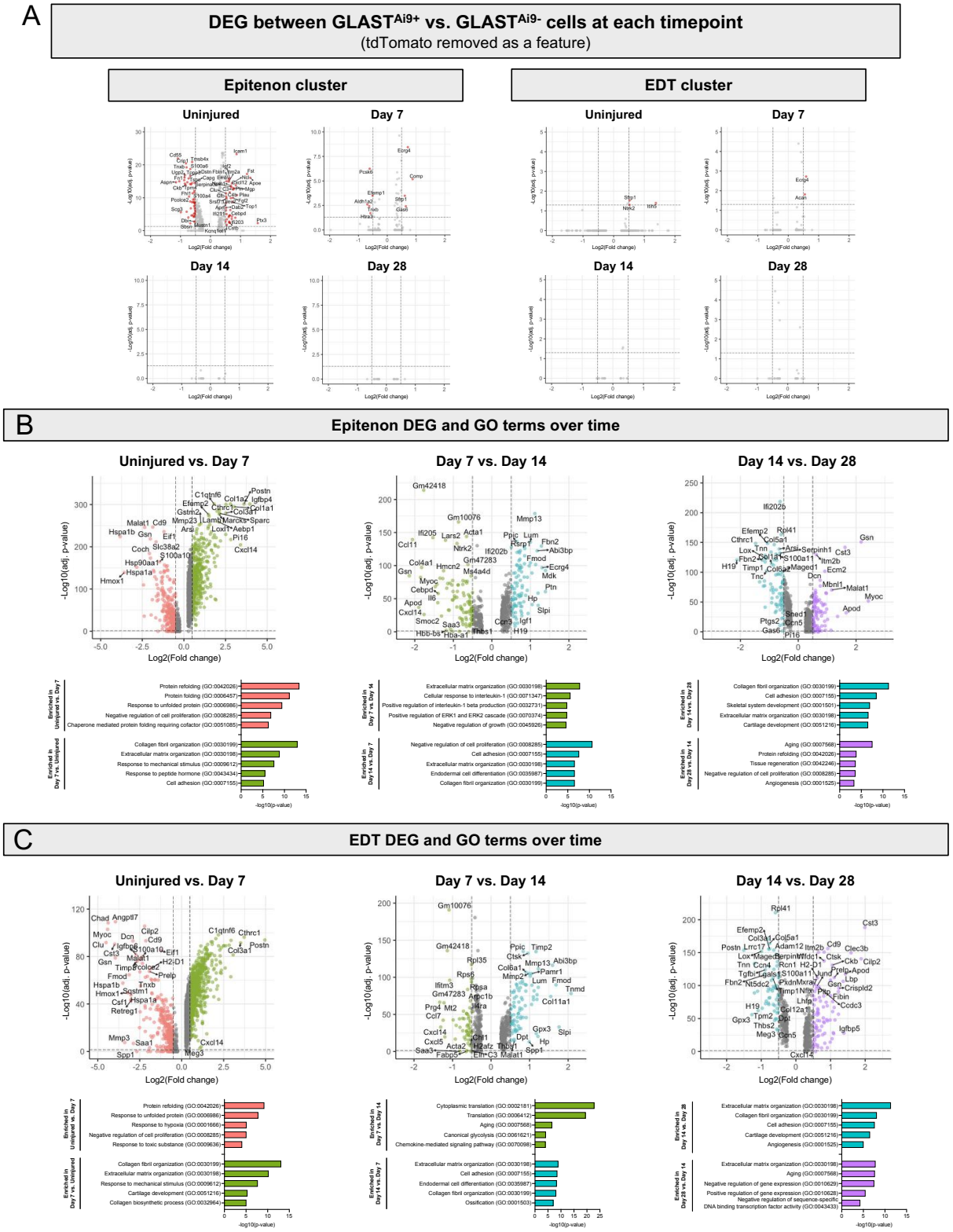

Fig. 4 supplement: (**A**) Volcano plots of differentially expressed genes (DEG) between GLAST^{Ai9}+ and GLAST^{Ai9}- in the epitenon and EDT clusters. tdTomato was removed as a feature for visualization. (**B**) Comparisons of DEG from different timepoints in the epitenon cluster (volcano plots) and GO term analysis for biological processes enriched at each timepoint (bar graphs). (**C**) Comparisons of DEG from different timepoints in the EDT cluster (volcano plots) and GO term analysis for biological processes enriched at each timepoint (bar graphs).

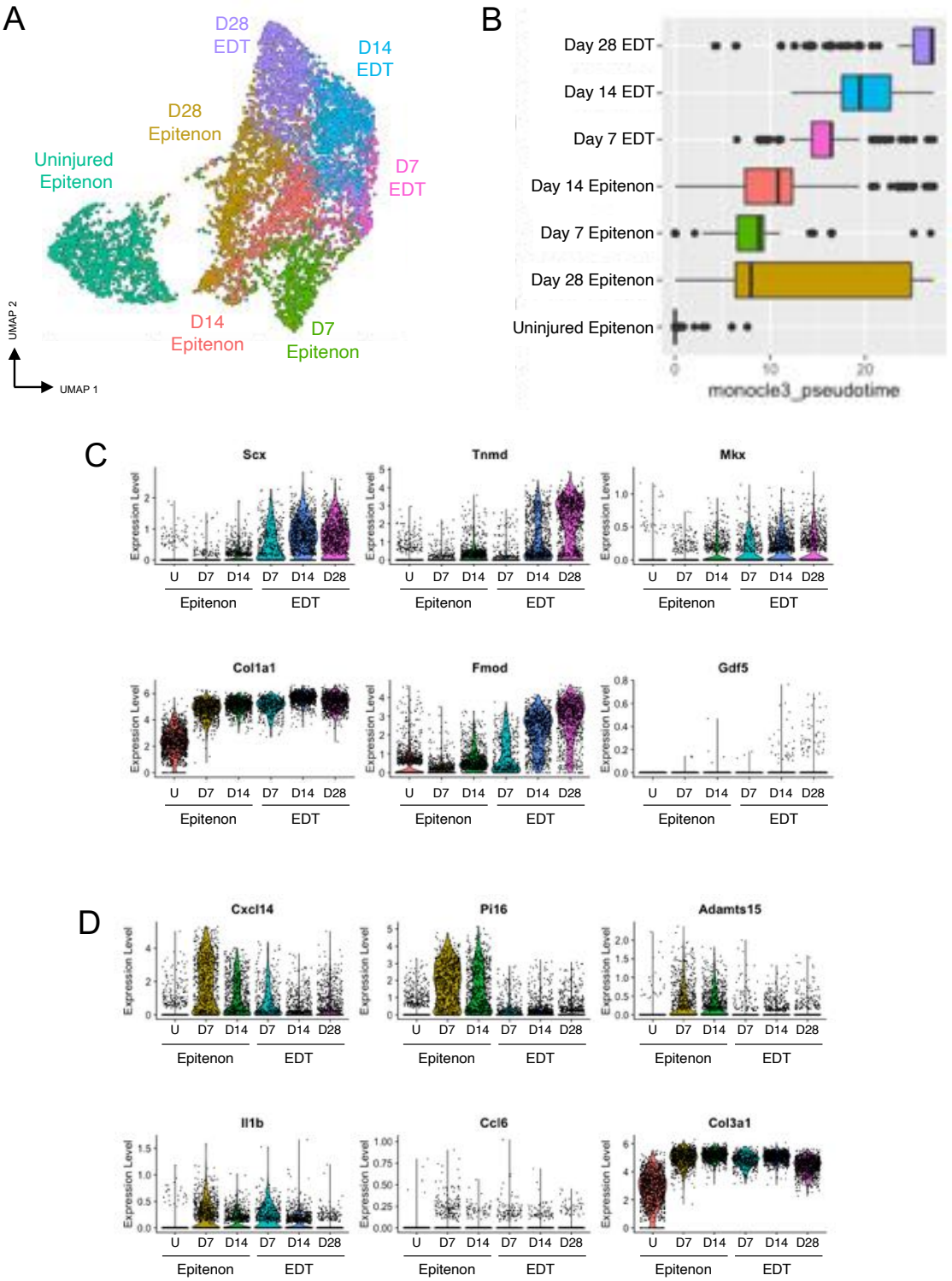

Fig. 5 supplement: (**A**) UMAP plot of sub-setted epitenon and EDT clusters for pseudotime trajectory analysis, including the day 28 (D28) epitenon cluster. (**B**) Bar graph of clusters from (**A**) showing distribution of cells in each cluster over pseudotime. Violin plots of (**C**) tenogenic and (**D**) fibrotic marker expression in real time post-injury.

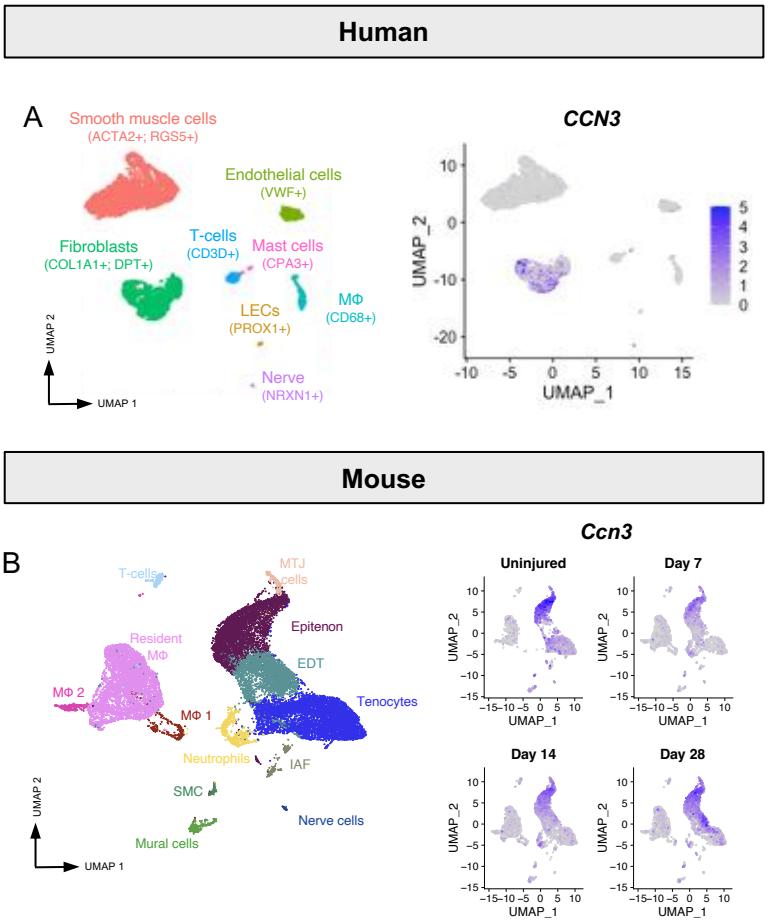

Fig. 6 supplement: (**A**) Annotated UMAP plot (left) and feature plot showing expression of *CCN3* (right) in the human peritendinous scar scRNA-seq dataset. (**B**) Annotated UMAP plot (left) and feature plot showing expression of *Ccn3* (right) in the mouse healing scRNA-seq dataset at each timepoint.